Original Article

Cell culture expansion media choice affects secretory, protective and immuno-modulatory features of adipose mesenchymal stromal cell-derived secretomes for orthopaedic applications

Enrico Ragni [a], Andrea Papait [b, c], Michela Maria Taiana [a], Paola De Luca [a], Giulio Grieco [a], Elsa Vertua [d], Pietro Romele [d], Cecilia Colombo [a], Antonietta Rosa Silini [d], Ornella Parolini [b, c], Laura de Girolamo [a, *]

[a] IRCCS Ospedale Galeazzi - Sant'Ambrogio, Laboratorio di Biotecnologie Applicate all'Ortopedia, Via Cristina Belgioioso 173, 20157 Milano, Italy
[b] Dipartimento di Scienze della Vita e Sanità Pubblica, Università Cattolica del Sacro Cuore, 00168 Roma, Italy
[c] Fondazione Policlinico Universitario Agostino Gemelli IRCCS, 00168, Roma, Italy
[d] Centro di Ricerca "E. Menni", Fondazione Poliambulanza Istituto Ospedaliero, 25124 Brescia, Italy

ARTICLE INFO

ABSTRACT

Introduction: Mesenchymal stromal cells (MSCs) gained attention for their anti-inflammatory and trophic properties, with musculoskeletal diseases and osteoarthritis (OA) being among the most studied conditions. Alongside cells, their released factors and extracellular vesicles (EVs), overall termed "secretome", are actively sifted being envisioned as the main therapeutic actors. In addition to standard supplementation given by foetal bovine serum (FBS) or human platelet lysate (hPL), new good manufacturing practice (GMP)-compliant serum/xeno (S/X)-free media formulations have been proposed, although their influence on MSCs phenotype and potential is scarcely described. The aim of this study is therefore to evaluate, in the OA context, the differences in secretome composition and potential after adipose-MSCs (ASCs) cultivation in both standard (FBS and hPL) and two next generation (S/X) GMP-ready supplements.
Methods: Immunophenotype and secretory ability at soluble protein and EV-related levels, including embedded miRNAs, were analysed in the secretomes by means of flow cytometry, nanoparticle tracking analysis, high throughput ELISA and qRT-PCR arrays. Secretomes effect was tested in *in vitro* models of chondrocytes, lymphocytes and monocytes to mimic the OA microenvironment.
Results: Within a conserved molecular signature, a divergent fingerprint emerged for ASCs' secretomes collected after expansion in standard FBS/hPL or next-generation S/X formulations. Regarding soluble factors, a less protective feature for those in the secretome collected after ASCs were cultured in S/X media emerged. Moreover, the overall message for EV-miRNAs was characterized by a preponderance of protective signals in FBS and hPL conditions in a context of general safeguard given by ASCs released molecules. This dichotomy was reflected on secretomes' potential *in vitro*, with expansion in hPL resulting in the most effective secretome for chondrocytes and in FBS for immune cells.
Conclusions: These data open the question about the implications from using new media for MSCs expansion for clinical application. Although the undeniable advantages for GMP compliant processes, this study results suggest that new media formulations would deserve a deep characterization to drive the choice of the most effective one tailored to each specific application.

---

* Corresponding author.
E-mail addresses: enrico.ragni@grupposandonato.it (E. Ragni), andrea.papait@unicatt.it (A. Papait), michelamaria.taiana@grupposandonato.it (M.M. Taiana), deluca.paola@grupposandonato.it (P. De Luca), giulio.grieco@grupposandonato.it (G. Grieco), elsa.vertua@poliambulanza.it (E. Vertua), pietro.romele@poliambulanza.it (P. Romele), cecilia.colombo@grupposandonato.it (C. Colombo), antonietta.silini@poliambulanza.it (A.R. Silini), ornella.parolini@unicatt.it (O. Parolini), laura.degirolamo@grupposandonato.it (L. de Girolamo).

1. Introduction

The use of biologic substances in orthopaedics (orthobiologics) is considered a novel and encouraging option to trigger tissue regeneration and to manage inflammation [1], as in osteoarthritis (OA) where cartilage degenerescence/degeneration and homeostasis imbalance are major traits [2]. Orthobiologics can be prepared from patient's tissues either at the point of care (POC) or in authorized facilities using more complex laboratory procedures [3]. Among the most used orthobiologics are platelet rich plasma (PRP) [4] and minimally manipulated cell-based therapies, such as those derived from adipose tissue (i.e. stromal vascular fraction - SVF, microfragmented adipose tissue - mFAT) [5] and bone marrow (bone marrow aspirate concentrate - BMAC) [6]. These therapies have been shown to be effective for OA, as recently reported by the European Society for Sports Traumatology, Knee Surgery and Arthroscopy (ESSKA). Through the creation of the Orthobiologic Initiative (ORBIT), ESSKA released a formal consensus addressing the use of injectable blood-derived products [7] and cell-based therapy (CBT) products [8]. CBT properties were mostly ascribed to their content of mesenchymal stromal cells (MSCs), also called medicinal signalling cells due to their ability to secrete bioactive factors and extracellular vesicles (EVs) (altogether defining the "secretome") that are immunomodulatory and trophic [9]. For these reasons, clinical-grade expanded MSCs, also falling under the hat of effective CBT in the ESSKA ORBIT consensus, and/or their secretomes are now envisioned as empowered next generation therapeutics for OA [10]. Under this paradigm, at mid of 2024, more than 80 clinical studies are registered as recruiting, completed or terminated for OA (https://www.clinicaltrials.gov/, condition: osteoarthritis, other terms: mesenchymal stem cell). Although evidence is supportive of MSC protective effects [11], additional investigations on immunomodulatory and chondroprotective mechanisms of action are needed to increase their efficacy.

For clinical applications, MSCs or their secretomes have to be produced under good manufacturing practice (GMP) protocols [12], with the advantage to have a more standardized and characterized product with respect to POC products although less cost-effective and accessible in the clinical routine from the regulatory perspective. Among the challenges in transferring MSCs knowledge from bench to bedside, the choice of the supplements used for cell expansion is of relevance since they can heavily affect cell potential [13]. Basal medium is typically supplemented with foetal bovine serum (FBS), available from several suppliers with GMP-grade certifications. Nevertheless, FBS has several drawbacks [14], including the risk of the transmission of infections, the high content of xenogeneic proteins and the high degree of batch-to-batch variation. To overcome these concerns, human platelet lysate (hPL) has been introduced for cell expansion [15]. However, the possibility of transmitting blood-borne viruses remains, alongside with a lack of consensus on the standardization of method used for hPL production which affects batch-to-batch consistency. Given these limitations, very recently serum- and xeno-free (S/X) defined medium supplements have been introduced to support reproducible manufacturing protocols for producing consistent batches of MSCs [16]. Some of these supplements are already available for GMP protocols. The main challenge in selecting the most favorable supplement is that the majority of studies assessing the effects of culture media on MSCs have focused on single comparisons, addressing only the minimal criteria for MSC identification [17,18]. Additionally, the impact of these supplements on secretome composition and therapeutic potential, especially when tailored to specific diseases, has not been thoroughly investigated.

The aim of this work was, therefore, to compare the secretome of adipose tissue-derived MSCs (ASCs) cultivated in FBS, hPL and two xeno-free media. An array of 200 cytokines, chemokines and growth factors, together with 784 miRNAs embedded in EVs, was studied in the frame of OA. Additionally, the effect of these secretomes on the cell types most involved in the OA phenotype such as chondrocytes, T cells and monocytes was evaluated. Outcomes are intended to shed light on the most favourable supplement for ASCs expansion and secretome collection for OA-driven therapeutic approaches.

2. Materials and methods

2.1. Human specimens collection and adipose-derived mesenchymal stromal cells (ASCs) isolation/expansion

Subcutaneous adipose tissue, purchased from Wepredic (Saint-Grégoire, France), was obtained from healthy females (age 32 yo ± 6, BMI 28 ± 3) undergoing aesthetic surgery procedures. ASCs were obtained as previously described [19]. Four media were used: i) DMEM/F12 + 10 % FBS (Thermofisher Scientific, Waltham, MA, USA), hereafter named condition F, supplemented with 1 % L-glutamine plus Penicillin-Streptomycin (PSG; Life Technologies, Carlsbad, CA, USA) and 1 % Fungizone (Life Technologies); ii) as in i) with 5 % human platelet lysate (hPL) in place of FBS (named H); iii) StemPro™ MSC SFM XenoFree (serum/xeno-free, cGMP compliant) (ThermoFisher, Waltham, MA, USA), 1 % PSG (named for sake of simplicity X1). Before seeding, flasks were coated with CELLstart™ Substrate (serum/xeno-free, cGMP compliant) (ThermoFisher) as per manufacturer's instruction; iv) StemFit® For Mesenchymal Stem Cells (xeno-free) (Amsbio, Cambridge, MA, USA), 1 % PSG (serum/named X2). Before seeding, flasks were coated with iMatrix-511 expressed in CHO cells for easier translation into GMP (Amsbio) as per manufacturer's instruction. iMatrix-511 is comprised of recombinant Laminin-511 E8 protein fragments. For X1 and X2 conditions, GMP-compliant recombinant trypsin (TrypLE™ Express) and PBS (CTS™ DPBS) (ThermoFisher) were used. After a week of expansion with an intermediate medium change, ASCs were detached and stored at −80 °C. When needed, to avoid differences given by culture conditions, all ASCs were seeded at the same time and further expanded with the same protocol (one week culture with intermediate medium change). This allowed to obtain around 90 % optical confluence in all media. Thus, experiments were performed after second passage.

PBMC from healthy volunteers were isolated via density gradient centrifugation (Histopaque 1077, Sigma−Aldrich, St. Louis, MO, USA), then frozen in FBS with 10 % DMSO (Merck) and stored in liquid nitrogen until use [20]. Three different PBMC donors were used for the immunomodulatory assays of ASC secretomes.

2.2. ASCs flow cytometry characterization

ASCs at 90 % confluence in the different media were detached and 100,000 cells were left unstained or stained with the following antibodies: anti-CD45-PE Vio770 clone REA747, CD73-PE clone REA804, CD90-FITC clone REA897 (Miltenyi Biotec, Bergisch Gladbach, Germany) and CD31-APC clone WM59, CD105-PerCP/Cy5.5 clone 43A3 and CD146-APC/Fire750 clone P1H12 (Biolegend, San Diego, CA, USA) in FACS buffer (1 x PBS, 2 % FBS, 1 mM EDTA) following manufacturer's protocol for Abs dilution. Incubations were performed at 4 °C for 30 min in the dark. After one wash in FACS buffer, at least 30,000 events were acquired with a CytoFLEX flow cytometer (Beckman Coulter, Fullerton, CA, USA).

2.3. ASCs secretome production

ASCs at 90 % confluence in the different media were washed twice with PBS to remove growth media contamination, detached and seeded at 1×10^6/ml in 24-well plates (0.5 ml per well) in DMEM/F12 supplemented with 1 % PSG and 1 % Fungizone for all conditions. After 4 days, the secretome was recovered, centrifuged at $300 \times g$ for 10 min at room temperature and eventually filtered with a 0.22 μm device. Aliquots were frozen at $-80\ °C$ until used for the experiments.

2.4. ELISA caharacterization of ASCs secretome

The enzyme-linked immunosorbent assay (ELISA) Quantibody® Human Cytokine Array 4000 Kit (RayBiotech, Peachtree Corners, GA, USA) was used to assay 1-fold diluted secretomes, following manufacturer's protocol. Only factors detected above their assay limits in all 12 samples or constantly missing in all 3 samples of one or multiple specific conditions and present in all the other samples were considered for analysis. After adjustment for the dilution factor, the values were reported in pg per exp6 ASCs.

2.5. Protein–protein interaction networks

Interactome maps of ELISA-identified proteins were generated with the online tool STRING (http://www.string-db.org, database v12.0) [21]. The following settings were used: (i) organism, *Homo sapiens*; (ii) meaning of network edges, evidence; (iii) active interaction sources, experiments and databases; (iv) minimum required interaction scores, low confidence (0.150).

2.6. ASC-extracellular vesicles (EVs) nanoparticle tracking analysis (NTA) characterization

Secretomes were 4-fold diluted and nanoparticle tracking analysis (NTA) run by Nanosight NS-300 system (NanoSight Ltd., Amesbury, UK) (5 recordings of 60 s). EVs were visualized with NTA software v3.4 providing both high-resolution particle size distribution profiles and concentration measurements.

2.7. ASC-EVs flow cytometry characterization

Secretomes were divided into aliquots, 8-fold diluted and left unstained, stained with 10 μM carboxyfluorescein succinimidyl ester (CFSE) for 1 h at 37 °C in the dark, or 10 μM CFSE followed by 30 min at 4 °C with the following antibodies, each used separately: anti-CD9-APC clone H19a, CD63-APC clone H5C6, CD73-APC clone AD2, CD81-APC clone 5A6 and CD90-APC clone 5E10. Samples were further 1-fold diluted (final 16-fold with respect to undiluted secretome) and at least 10,000 events were acquired with a Cyto-FLEX flow cytometer (Beckman Coulter) after calibration with FITC-fluorescent nanobeads (100, 160, 200, 300, 240, 500 and 900 nm; Biocytex, Marseille, France) used as internal control for efficient detection in the nanometric range.

2.8. ASC-EVs embedded miRNAs identification

Secretomes were 9-fold diluted in PBS for a total volume of 10 ml and ultra-centrifuged at $100,000 \times g$ for 9 h at 4 °C in an Optima L-90K Ultracentrifuge (Beckman Coulter, Brea, CA, USA) equipped with a Type 70.1 Ti Fixed-Angle Titanium Rotor (Beckman Coulter). RNA extraction, cDNA synthesis and qRT-PCR reaction were performed as previously described [19]. Eventually, the global mean method [22] allowed normalization between samples. ath-miR-159 spike-in was used to monitor whole procedure efficiency between samples and to assign a quantity to identified miRNAs comparing their normalized C_{RT} values with those obtained with ath-miR-159 corresponding to an input of 30 pg. Values are reported as pg of each miRNA per exp9 EVs calculated with NTA.

2.9. miRNAs targets identification

The mRNA targets of detected miRNAs were identified with miRTarBase (https://mirtarbase.cuhk.edu.cn/∼miRTarBase/miRTarBase_2022/php/index.php, database v9.0) [23]. Only miRNA-mRNA interactions supported by strong experimental evidence were considered.

2.10. Computational analyses

ClustVis package (https://biit.cs.ut.ee/clustvis/) [24] was used to generate principal component analysis (PCA) and hierarchical clustering plots. Maps were generated using the following settings: ln(x) or ln(x+1), when values close to 0 were present, transformation; no row centering; no unit variance scaling; PCA method: SVD with imputation. miRNAs targeting real hub genes were found by screening miRNet 2.0 [25]. Setting: Organism homo sapiens, ID type miRBase ID, Targets Genes (miRTarBase v8.0). The first 100 Enriched Reactome Pathways, Biological Processes and Molecular Functions terms were reported.

2.11. Secretomes effects on chondrocyte proliferation

Human immortalized chondrocytes (INS–CI-1006; InSCREENeX, Braunschweig, Germany) at passage 11 cultivated in DMEM/F12 + 10 % FBS (ThermoFisher) supplemented with 1 % PSG and 1 % Fungizone were seeded at 10,000 cells/cm² in 96-wells plates. After 8 h to allow for cells attachment, medium was removed from wells and chondrocytes were supplemented with 100 μl fresh complete medium (DMEM/F12 10 % FBS + 1 % PSG + 1 % Fungizone), fresh complete medium supplemented with 1 ng/ml Interleukin 1-beta (IL1B; Sino Biological, Eschborn, Germany) or secretomes 1-fold and 4-fold diluted in fresh complete medium with final 1 ng/ml IL1B supplementation. For wells with diluted secretomes, final FBS, PSG and Fungizone were 10 %, 1 % and 1 %, respectively. All samples were prepared in quadruplicate. Initial amount of cells was immediately measured in two wells of the quadruplicate removing the supernatants and adding 90 μl of fresh complete medium supplemented with 10 μl CCK-8 solution (Sigma–Aldrich, Darmstadt, Germany). Plates were incubated at 37 °C and absorbance read at 450 nm using a microplate reader (VICTOR™ X3, PerkinElmer, Waltham, MA, United States) at 15 min, 30 min and 1 h. To correct for background, wells without cells were prepared in duplicate and measured, and values subtracted to samples. Also, a calibration curve was performed with 10,000, 20,000, 40,000, 60,000 and 80,000 cells/cm² in 96-wells plates to compare absorbance values and assign a cell number for each well. After 48 h, remaining samples in duplicate were assayed with the identical protocol for CCK-8 and cell number was calculated based on the calibration curve. Proliferation was calculated comparing cell number at the beginning of the secretomes incubation with respect to samples at 48 h.

2.12. Secretomes effects on chondrocyte inflammation

Immortalized chondrocytes were prepared as previously described and seeded at 90,000 cells/cm² in 24-wells plates. Cells were incubated with fresh complete medium, fresh complete medium supplemented with 1 ng/ml Interleukin 1-beta or secretomes 1-fold and 4-fold diluted in fresh complete medium with final 1 ng/ml IL1B

supplementation. For wells with diluted secretomes, final FBS, PSG and Fungizone were 10 %, 1 % and 1 %, respectively. After 48 h, supernatants were removed and RNA extracted with RNeasy® Mini Kit (Qiagen), following manufacturer's instructions. cDNA was obtained with iScript™ cDNA Synthesis Kit (Bio-Rad Laboratories Srl, Segrate, Italy) and gene expression for CTSS, IL1/6/8, CCL5 and IDO was performed with iTaq Universal SYBR Green Supermix (Bio-Rad) in a CFX Opus Real-Time PCR System (Bio-Rad) using TBP and RPLP0 as reference genes. Primer sequences: CTSS (F:TCCTCTACAGAAGTGGTGTCTAC, R:AGCCAACCACAAGTACACCAT), IL1 (F:AGCTGGAGAGTGTAGATCCC AA, R:ACGGGCATGTTTTCTGCTTG), IL6 (F:ATCTGGATTCAATGAGGA-GACTTG, R:TTGTACTCATCTGCACAGCTC), IL8 (F:ACCGGAAGGAAC-CATCTCAC, R:GGCAAAACTGCACCTTCACAC), CCL5 (F:GGTACCATGAAG GTCTCCGC, R:GGTGTCCGAGGAATATGGGG), IDO (F:GCTAAAGGCGCTG TTGGAAA, R:TTGCCTTTCCAGCCAGACAAA), TBP (F:GCCACGCCAGCTT CGGAGAG, R:CCGCAGCAAACCGCTTGGGA), RPLP0 (F:TGTGGGCTCCAA GCAGATGCA, R:GCAGCAGTTTCTCCAGAGCTGGG).

2.13. T-cell proliferation

T-cell proliferation assays were conducted by stimulating PBMCs with an anti-CD3 monoclonal antibody. PBMCs (1×10^5/ well in a 96-well plate) were activated with 125 ng/ml (final concentration) anti-CD3 (Orthoclone OKT3; Janssen-Cilag, Cologno Monzese, Italy). Activated PBMCs (PBMC + anti-CD3) were cultured in the presence of the different ASCs secretomes. Various volumes of secretome were tested (10, 50, or 100 μl/well of secretome, corresponding to 5 %, 25 %, or 50 %, respectively, of the final volume) for a duration of 3 days, with the final volume of each well set at 200 μl. Control conditions included activated PBMCs cultured alone, and all experiments were performed in triplicate in RPMI 1640 medium (Cambrex, Verviers, Belgium) supplemented with 10 % heat-inactivated FCS, 2 mM L-glutamine, and penicillin/streptomycin. T-cell proliferation was assessed using 5-ethynyl-2′-deoxyuridine (EdU) incorporation, as described previously [26]. Briefly, 10 μM EdU (Life Technologies) was added to PBMCs at day 3 post-stimulation. After 16−18 h, cells were harvested and EdU incorporation was evaluated by adding 2.5 μM 3-azido-7-hydroxycoumarin (Jena Biosciences, Jena, Germany) in a buffer solution (100 mM Tris−HCl pH 8.0, 10 mM L-ascorbic acid, 2 mM $CuSO_4$) at room temperature for 30 min. Cells were acquired using a FACSymphony A3 (BD Biosciences, Franklin Lakes, NJ, USA), and the percentage of proliferating EdU-positive cells was analysed with FlowJo V10 (BD Biosciences). Additionally, cells were stained with eFluor 780 (ThermoFisher) for the exclusion of dead cells.

2.14. $CD4^+$ T-cell differentiation

The phenotypic characterization was conducted using flow cytometry analysis to evaluate the expression of specific cell surface markers and transcription factors for identifying T helper subsets (Th1, Th2, and Th17) and regulatory T cells (Treg). Peripheral blood mononuclear cells (PBMCs), stimulated with anti-CD3, were cocultured for 5 days with the different ASCs secretome. After centrifugation, cells were collected and stained with antibodies anti-CD3 BUV496 (SK7), CD4 FITC, CD45RA BUV395 (HI100), CD196 BV421 (11A9), CD183 BB700 (1C6/CXCR3), CD25 APC-R700 (M-A252), and FoxP3 PE-CF594 all purchased from BD Biosciences, and CD194 PE-Vio770 (REA279) (Miltenyi). The staining was performed by incubating cells with the mix of antibodies for 30 min in the dark at 4 °C. eFluor 780 staining (BD Biosciences) was performed to exclude dead cells. T-cell subsets were identified through a sequential gating strategy, initially identifying T effector cells as CD4+CD45RA− cells. Subsequent identification of different T

helper (Th) subsets was as follows: Th1 as CD196−CD183+, Th17/ Th1 as CD196+CD183+, Th17 as CD183-CD196+CD194+ and Th2 as CD196−CD183−CD194+. Alternatively, Treg polarization was induced in a mixed lymphocyte reaction (MLR-T) by co-culturing T cells (1×105, isolated with the Pan Isolation Kit, Miltenyi) with 1×105 gamma-irradiated allogeneic PBMCs. Co-culture in the absence or presence of different secretomes (100, 50, or 10 μL/well; 50 %, 25 %, or 5 %, respectively, of the final volume), was performed. Treg polarization was evaluated after 6 days of co-culture through intracellular staining for FoxP3, performed after fixation and permeabilization using BD Cytofix/Cytoperm, followed by staining with anti-FoxP3 antibody. Data were acquired using a FACSymphony A3 and analysed with FlowJo V10 (BD Biosciences), with T effector cells initially identified as CD4+CD45RA-. Tregs were then assessed as a percentage of CD25highFoxP3+ cells.

2.15. Monocyte maturation and differentiation towards mDC

Mature dendritic cells (mDCs) were generated from 2.5×10^5 PBMCs cultured in 48-well plates (Corning; Corning, New York, NY, USA) for 4 days. The culture medium consisted of 0.5 ml RPMI 1640 complete medium supplemented with 50 ng/ml recombinant human IL-4 (R&D Systems, Minneapolis, MN, USA) and 50 ng/ml granulocyte-macrophage colony-stimulating factor (GM-CSF). Complete maturation was achieved by adding 0.1 μg/ml lipopolysaccharide (LPS) for additional 2 days. mDCs were harvested after 6 days of differentiation, in the absence or presence of 50 or 100 μl/well of secretome (representing 10 % or 20 %, respectively, of the final volume). Various secretome products were added at day 0, coinciding with the initiation of the differentiation protocol. Phenotypic analysis was performed using flow cytometry. Prior to surface marker staining, cells were treated with eFluor 780 for dead cell exclusion, and CD3-positive cells were excluded from the analysis. Staining was conducted for CD197 A647 (clone 3D12), CD14 BUV395 (clone MΦP9), CD163 bv421 (clone ghi/61) and CD1a BV480 (clone HI149) (BD Biosciences) by incubating cells with the mix of antibodies for 30 min in the dark at 4 °C. Samples were acquired using a FACSymphony A3 and analysed with FlowJo V10 (BD Biosciences).

2.16. Statistical analyses

Data are expressed as mean ± SD unless otherwise indicated. Data are visualized in violin-truncated plots incorporating Tukey variations. Comparative analysis of parameters was performed using both one-way and two-way analyses of variance (ANOVA). Only for PBMCs proliferation, a supplementary a Student's t-test for direct comparison was performed. Normal data distribution was assessed by the Shapiro−Wilk normality test (α of 0.01). The findings represent a minimum of three independent experiments. Statistical analyses were conducted using Prism 8 software (GraphPad Software, La Jolla, CA, USA), applying a significance threshold of p ≤ 0.05. Values below this threshold were considered statistically significant.

3. Results

3.1. ASCs characterization and immunophenotype

At 90 % optical confluence, ASCs cultivated in the four analysed media showed different cell density: 6.1×10^3 cells/cm^2 ± 0.9 in F, 37.8 ± 12.2 in X1, 47.6 ± 1.3 in X2 and 14.2 ± 1.2 in H. Significant (p-value ≤0.05) dichotomy was reached for F vs X1 or X2 and H vs X1 or X2. ASCs cultivated in F were highly positive for the presence of

MSCs markers CD73 and CD90, while CD105 and CD146 had a lower expression although their presence in the whole cell population allowed for a homogeneous peak shift in the cytograms (Fig. 1A and B). Hemato-endothelial markers CD45 and CD31 were not present, confirming ASCs identity. The culture in hPL and even more in both xeno-free media resulted in a significant decrease of CD105 expression, alongside with an increase of CD146 in X1/X2 (Fig. 1B and C). Once compared, ASCs in X1 or X2 did not show differences for any of the tested surface markers.

3.2. ASCs secreted factor dependence on culture conditions

Regardless of the media used to cultivate ASCs, 37 factors could be detected in the analysed secretomes (Additional file 1 and Table 1A), with IL23A not detected in F and X1 conditions. Considering the average quantities, the most abundant proteins ($\geq$10,000 pg/10^6 ASCs) were IGFBP4/3, VEGF, TIMP1/2 and IL6. Other 12 factors had an average amount between 1000 and 10,000 pg/10^6 ASCs. Functional protein association network analysis based on experimental and database-annotated interactions allowed the definition of a main cluster enriched in growth factors, cytokines and their receptors (including VEGF, CSF1, EGFR, HGF, TGFB1, FGF2, IL23A, IL6, IL6ST, KIT, KDR, FLT3LG and FLT4). EGFR is a key hub for other growth factors-related proteins and receptors such as IGFBP2/3/6 or TNFRSF1A/B, FAS and IL1RN, respectively. Other 2 IGFBPs (1/4) were also connected to the main cluster. Of note, in the frame of the pathology herein investigated, several factors related to musculoskeletal disorders were included in the list (Disease Ontology DOID:17 — Musculoskeletal system disease — FDR 0.73E-4), supported by those linked to both extracellular matrix (Reactome Pathway HSA-1474244 — Extracellular matrix organization - FDR 2.39E-5; Gene Ontology GO:1903053 — Regulation of extracellular matrix organization — FDR 3.30E-4) and immune/inflammatory response (GO:0006955 - Immune response — FDR 9.54E-7; GO:0006954 - Inflammatory response — FDR 2.99E-9). Among the most relevant OA-related immune cells (Fig. 2B), 7 proteins were involved in Regulation of T cell proliferation (GO:0042129, FDR 7.88E-6), 8 in Regulation of T cell activation (GO:0050863, FDR 4.36E-5) and 3 in Regulation of macrophage differentiation (GO:0045649, FDR 8.90E-3) or 2 in chemotaxis (GO:0010758, FDR 3.96E-2).

To score differences due to culture media, a correlation analysis for the factors released by the three ASCs donors cultivated under the same condition to test their homogeneity was performed. r Pearson resulted to be very high, namely 0.93 $\pm$ 0.05 for F, 1.00 $\pm$ 0.00 for X1, 0.98 $\pm$ 0.01 for X2 and 0.93 $\pm$ 0.03 for H. Comparing conditions, the lowest r emerged for factors released by ASCs pre-cultured in FBS (0.54 $\pm$ 0.20 for F vs H, 0.43 $\pm$ 0.17 for F vs X1, 0.42 $\pm$ 0.18 for F vs X2), while the correlation values were higher for the other three media (0.96 $\pm$ 0.04 for H vs X1, 0.95 $\pm$ 0.04 for H vs X2 and 0.99 $\pm$ 0.01 for X1 vs X2). Of note, the top of the rankings ($\geq$10,000 pg/10^6 ASCs) was quite homogeneous with 6 out of 6 identical proteins for F and X1, and 5 out of 6 for X2 and H. Nevertheless, a few significantly different ($\geq$2 fold, p-value $\leq$0.05) molecules laid within this group (Table 1B). In particular, IGFBP3 was always more expressed in X1 (6.3 vs F, 5.4 vs X2 and H), as well as TIMP2 (3.3 vs H, 2.4 vs X2 and 2.0 vs F). The same trend was observed also for PLAUR (3.0 vs X2, 2.9 vs H and 2.4 vs F), in 10th position of the overall ranking. X1 also had higher amount for the 9th position holder INHBA (15.8 vs X2 and 9.7 vs H), together with VEGF and the moderately expressed GDF15 (3.2 and 2.0 vs X2, respectively). Other low abundance proteins resulted modulated, usually being more released in F and/or X1 (CSF1, IL1RN and FLT3LG).

3.3. ASC-EVs characterization and immunophenotype

The highest release of EVs per cell occurred in ASCs pre-cultured in FBS (4.1 $\times$ 10^3 $\pm$ 0.8), with all the other conditions leading to a significant reduced amount (2.8 $\times$ 10^3 $\pm$ 0.5 for H with p-value of 0.0541, 2.4 $\pm$ 0.1 for X1 and 1.7 $\pm$ 0.1 for X2) (Fig. 3A). EVs secreted by ASCs pre-grown in FBS also had the largest size, being 148 nm $\pm$ 7 vs 135 $\pm$ 7 for X1, 126 $\pm$ 3 for H and 110 $\pm$ 2 for X2 (Fig. 3B). X2 and H EVs resulted significantly different from F, as X1 vs X2. Flow cytometry clearly confirmed the NTA data regarding size range (around 100–200 nm) of EVs when compared to nano-metric beads (Fig. 3C). Moreover, the analysis showed a very low signal for CD9 presence, with a homogeneous albeit very faint peak shift, while both EVs markers CD63/81 and MSCs markers CD73/90 were present at high levels (Fig. 3C and D), without relevant differences among the conditions.

3.4. ASCs EV-miRNAs dependence on culture conditions

Regardless of the culture media used for ASCs expansion, 157 miRNAs could be detected in the analysed EVs (Additional file 2). To further sharpen data significance, only those miRNAs falling in the first quartile of expression in each of the analysed samples were further processed, for a total of 49 candidates (Additional file 3 and Table 2A). Performing a miRNA-centric network analysis scoring validated target genes, several biological pathways emerged (Additional file 4A), where the most significant ones (p-value $\leq$ E−20) were related to Gene expression, Cell cycle, Cellular response to stress, Disease and Oxidative stress/Senescence. Consistently, among the most enriched biological processes several gene ontology terms related to cell division and mitosis were found (Additional file 4B), corroborated by the most significant ones for molecular functions related to nucleotide binding (Additional file 4C).

To get a more focused analysis on media effect on specific EV-miRNAs abundance, a correlation study was performed on candidates falling in the first quartile of detection. r Pearson resulted to be 0.96 $\pm$ 0.01 for F samples, 0.82 $\pm$ 0.05 for X1, 0.85 $\pm$ 0.10 for X2 and 0.97 $\pm$ 0.01 for H. Comparing conditions, F and H resulted the most similar (0.92 $\pm$ 0.04), as confirmed by comparable difference with respect to X1 (0.62 $\pm$ 0.09 for both F and H) and X2 (0.13 $\pm$ 0.12 for F and 0.04 $\pm$ 0.08 for H). X1 and X2 also had low correlation (0.29 $\pm$ 0.17). These results were confirmed by the number of modulated miRNAs (Table 2B). The highest number of significantly different miRNAs were found comparing F vs X2 and H vs X2 (28 and 23, respectively), followed by F vs X1 and H vs X1 (19 and 18, respectively). As expected, F vs H were very similar, with only 4 different miRNAs. Of note, although with a low r, the couple X1 vs X2 was characterized by only 2 modulated molecules, suggesting a general fluctuation instead of few highly diverging players in a context of a conserved pattern. Focusing at single miRNAs, several had a superimposed arrangement such as those showing a significant upregulation in both F and H vs X1 or X2 (miR-125b-5p, miR-100-5p, mir-99a-5p, miR-26a-5p, miR-29a-5p, miR-99b-5p, miR-127-3p, miR-10a-5p and miR-143-3p) or others having the complete reverse behaviour (miR-193b-3p, miR-214-3p, miR-320a-3p and miR-574-3p). Similar to the first group, miR-222-3p and miR-31-5p were more abundant in H vs X1/2 and F vs X2, while similar to the last group, miR-92a-3p and miR-197-3p were more present in X2 vs F/H and X1 vs F. let-7b-5p and let-7e-5p were upregulated in F vs all the other conditions. miR-194-5p and miR-218-5p were more present in X2 vs H or F, while miR-224-5p was the opposite. These data of conserved trends for groups of miRNAs able to shape the four EV-miRNAs fingerprints were corroborated by PCA and hierarchical clustering (Fig. 4A and B). The heat map
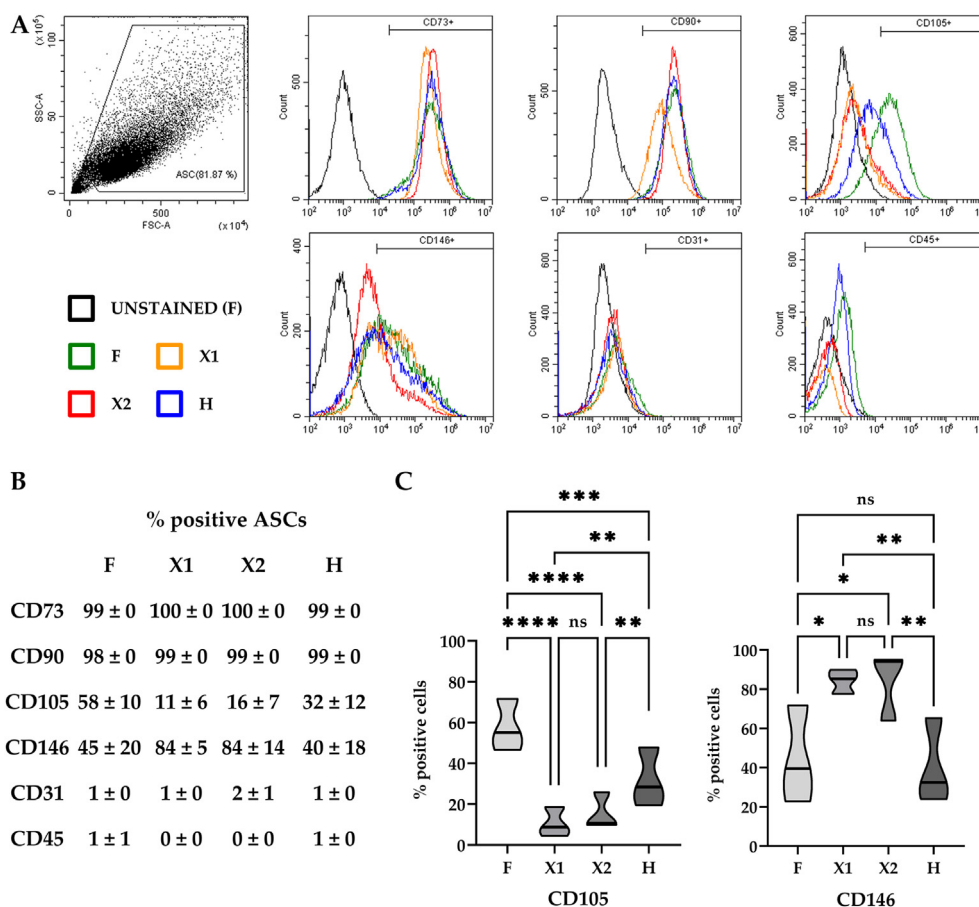
Fig. 1. ASCs immunophenotype. A) Cytograms of markers tested in a representative ASCs cultivated in the four conditions of the study. Unstained sample represents ASCs cultivated in FBS (condition F). B) Percentage of positive ASCs for both MSCs (CD73/90/105/146) and hemato-endothelial (CD31/45) markers (mean ± SD, N = 3 independent experiments). C) Significant differences for CD105 and CD146 between ASCs in the four media. (median (thick line) and 25th and 75th quartiles; *p ≤ 0.05, **≤ 0.01, ***p ≤ 0.001, ****p ≤ 0.0001; N ≥ 3 independent experiments).

showed F and H conditions under the same cluster, as well as X1 and X2 although, as per lower *r*, with a higher height of bars meaning a greater distance. This was evident in the PCA plot where X1 and X2 laid at greater distance with respect to F and H that grouped close.

Eventually, to weight at global level the additional effect of single miRNA modulations, for each candidate the target mRNAs referring to those molecules being reported to be regulated in OA tissues [27] was extracted (Table 2C). For each of the identified targets, a weight given by all miRNAs regulating those transcripts was calculated (Table 3). As for the single miRNAs, F *vs* X2 and H *vs* X2 resulted the comparisons with the highest number of significantly different factors (27 and 20, respectively), followed by F *vs* X1 and H *vs* X1 (16 and 14, respectively). As expected, X1 *vs* X2 and F *vs* H had only few differentially targeted proteins (3 and 1, respectively). Focusing at single factors, several had an overlapping pattern such as those displaying a significant increased targeting in both F and H *vs* X1 or X2 (LIF, EPO, CXCL12, TGFB3, MMP13, MMP1, IL1RL, MMP3, ADAMTS9 and ADAMTS4). An identical trend was observed also for ADAMTS9 and 4, alongside a concomitant upregulation for X1 *vs* X2 or F *vs* H, respectively. Similar to these factors, MMP2 and APC were more targeted in F *vs* X1/2 and H *vs* X2, or TIMP2 in H *vs* X1/2 and F *vs* X2. CTSB had an opposite regulation with higher targeting in X1/2 *vs* F and X2 *vs* H. CCL5 was less targeted in F *vs* X1/2, while KITLG in X1/2 *vs* H. Four proteins were specific for F/H *vs* X2 (EGF, FGF1 and TIMP3, more targeted; PLAU,

less targeted). BDNF had a similar pattern, more targeted in F/H/X1 *vs* X2. Of note, 7 factors were specific for F *vs* X2 (WNT1, TGFB2, PDGFB, HGF, MMP9 and PLAT, more targeted; TIMP1, less targeted), 1 for F *vs* X1 (IGF2, more targeted) and 2 for H *vs* X1 (IL2, less targeted; ADAM12, more targeted). Overall, at EV-miRNA level, F and H conditions appeared to have a stronger and positive impact on OA factors.

3.5. Effect of secretome on human chondrocytes

The effect of the four secretomes on human chondrocytes was tested in cells treated with IL1β, a well-described model of inflammation commonly used as the first step in evaluating new therapeutic approaches on OA-like phenotype management [28]. X1 secretome at 1:1 dilution was the only one able to significantly (p-value ≤0.05) reduce cell growth with respect to both standard and inflamed chondrocytes, which did not differ from each other (Fig. 5A). Noteworthy, a dose response was present, since 1:4 dilution did not result in any change. The value of cell proliferation under X1 condition was significantly lower than those in X2 (both 1:1 and 1:4) and H (only 1:1), and F (only 1:4). In addition, F samples at 1:1 dilution were able to reduce chondrocyte growth when compared to CTRL, although at a lesser extent than X1. Thus, more concentrated secretomes appeared to have an effect, when present (F and X1), on chondrocytes and therefore for gene expression analysis this experimental condition (1:1) was analysed.

Table 1
ASCs released factors after cultivation in the 4 media of the study.

A - pg/10⁶ ASCs						B - FOLD						
PROTEIN	F	X1	X2	H	MEAN	F vs X1	F vs X2	F vs H	X1 vs X2	X1 vs H	X2 vs H	DESCRIPTION
IGFBP4	16509	692237	427330	242525	344650	0.02 *						Insulin-like growth factor-binding protein 4
IGFBP3	9796	61999	11488	11478	23690	0.2 ****			5.4 ****	5.4 ****		Insulin-like growth factor-binding protein 3
VEGF	23965	33221	10505	15540	20808				3.2 *			Vascular endothelial growth factor A
TIMP2	11501	22819	9484	6865	12667	0.5 *			2.4 **	3.3 **		Metalloproteinase inhibitor 2
TIMP1	11208	15600	9604	8375	11196							Metalloproteinase inhibitor 1
IL6	14371	14948	3947	7833	10275							Interleukin-6
IGFBP6	6912	12438	8895	5918	8541							Insulin-like growth factor-binding protein 6
SERPINE1	7871	9164	5279	7743	7514							Plasminogen activator inhibitor 1
INHBA	8990	11397	719	1170	5569				15.8 *	9.7 *		Inhibin beta A chain
PLAUR	4229	10357	3460	3522	5392	0.4 ***			3.0 ***	2.9 ***		Urokinase plasminogen activator surface receptor
MIF	6689	2777	4283	5154	4726							Macrophage migration inhibitory factor
BMP7	5994	7334	2073	2914	4579							Bone morphogenetic protein 7
IGFBP1	2123	208	7416	7854	4400							Insulin-like growth factor-binding protein 1
TNFRSF1A	3001	3830	2709	2714	3063							TNF receptor superfamily member 1A
IGFBP2	277	2847	4168	4269	2890							Insulin-like growth factor-binding protein 2
HGF	174	3057	2364	1659	1813							Hepatocyte growth factor
IL6ST	624	981	1245	1561	1103							Interleukin-6 receptor subunit beta
GDF15	1089	1406	694	872	1015				2.0 **			Growth/differentiation factor 15
CD14	556	349	252	2820	994							Monocyte differentiation antigen CD14
EGFR	1752	355	452	540	775							Epidermal growth factor receptor
ALCAM	1517	356	570	327	693							CD166 antigen
CCL2	825	834	395	454	627							C—C motif chemokine 2
TNFRSF1B	729	593	233	827	596							TNF receptor superfamily member 1B
IL23A	0	0	852	814	417							Interleukin-23 subunit alpha
FGF2	1001	22	186	447	414							Fibroblast growth factor 2
TGFB1	36	51	709	759	389							Transforming growth factor beta-1
ANG	70	618	499	358	386							Angiogenin
CTSS	214	425	229	447	329							Cathepsin S
TNFRSF11B	447	57	167	164	209							TNF receptor superfamily member 11B
CSF1	350	217	115	146	207		3.0 **	2.4 *				Macrophage colony-stimulating factor 1
FAS	267	346	103	72	197							TNF receptor superfamily member 6
KDR	117	274	89	155	159	0.4 **			3.1 **			Vascular endothelial growth factor receptor 2
IL1RN	299	137	51	97	146	2.2 **	5.8 ****	3.1 ***	2.7 *			Interleukin-1 receptor antagonist protein
TNFRSF21	28	120	117	65	82							TNF receptor superfamily member 21
FLT3LG	23	14	4	2	11		6.1 **	12.9 ***	3.8 *	8.1 *		Fms-related tyrosine kinase 3 ligand
KIT	13	7	8	13	10							Mast/stem cell growth factor receptor kit
FLT4	13	13	6	7	10							Vascular endothelial growth factor receptor 3

Released ASCs factors ordered by mean, from most to less abundant factor, obtained from the four conditions. For each fold ≥2 or ≤0.5 the significance is shown: * for p-value ≤0.05, ** ≤0.01, ≤ *** 0.001 and **** ≤0.0001. N = 3.

Six genes involved in inflammation-dependent OA phenotype at different levels (Chatepsin S (*CTSS*) for matrix remodelling; Interleukins (*IL1/6/8*) as inflammatory cytokines; C—C Motif Chemokine Ligand 5 (*CCL5*) as inflammatory chemokine and indoleamine 2,3 dioxygenase 1 (*IDO1*) as Wnt pathway activator and cartilage regeneration blocker) were tested (Fig. 5B and C). It clearly emerged that all secretomes were able to reduce the inflammatory activation given by IL1β, although with some differences. H condition resulted the best performer, being the only one that showed no significant difference with respect to CTRL for at least one gene (*CTSS*). Moreover, H resulted significantly lower than all the other conditions for *IL6* and *IL8*, than X2 for *CTSS* and X1 for *IL1*. Between the other secretomes, only F showed some differences, reducing the expression of *IL1* and *IL8* with respect to X1. Thus, in a context of efficacy for all secretomes, H and at a lesser extent F resulted the conditions giving the most effective modulation on inflamed chondrocytes.

3.6. Secretome effect on immune cells

ASC-derived secretomes were tested for their immunomodulatory properties. First, we focused on evaluating the secretome capacity to influence the activation and proliferation of PBMCs following anti-CD3 stimulation (Fig. 6A). Although without reaching a statistical significance, the highest inhibitory effect on T-cell activation and expansion emerged supplementing PBMCs with F secretome, where a decrement in effectiveness was evident through the observed titration loss. Only in this condition, a Student's t-test allowed to reach significance for the two highest concentrations *vs* control (PBMC + anti-CD3). Second, we next sought to explore secretome potential on adaptive immunity by scoring their influence on the differentiation of CD4 T lymphocytes. Of note, a low albeit not significant variation was observed in Treg subset for H, with an increased polarization (Fig. 6B). Also, for all analysed T helper subsets (Th1/2/17) no significant differences emerged, with only a trend towards downregulation for Th1 for F (Fig. 6C). Third, we analysed the ability of the secretomes to modulate the polarization of monocytes towards mDCs. F condition was the ablest to affect monocyte differentiation, followed to a lower extent by X1 and H, while X2 did not show almost any effect. This was evident in the F-dependent maintenance of pro-monocytic marker CD14 expression, which is downregulated in mDCs (Fig. 7A). Additionally, a downregulation of differentiation markers CD1a and CD197, albeit not significant for this molecule, was observed for both tested concentrations of F, while for X1 and H only the highest concentration resulted effective (Fig. 7B and C). This higher immunomodulatory action for F was also reflected in the reduced, although not significant, downregulation of co-
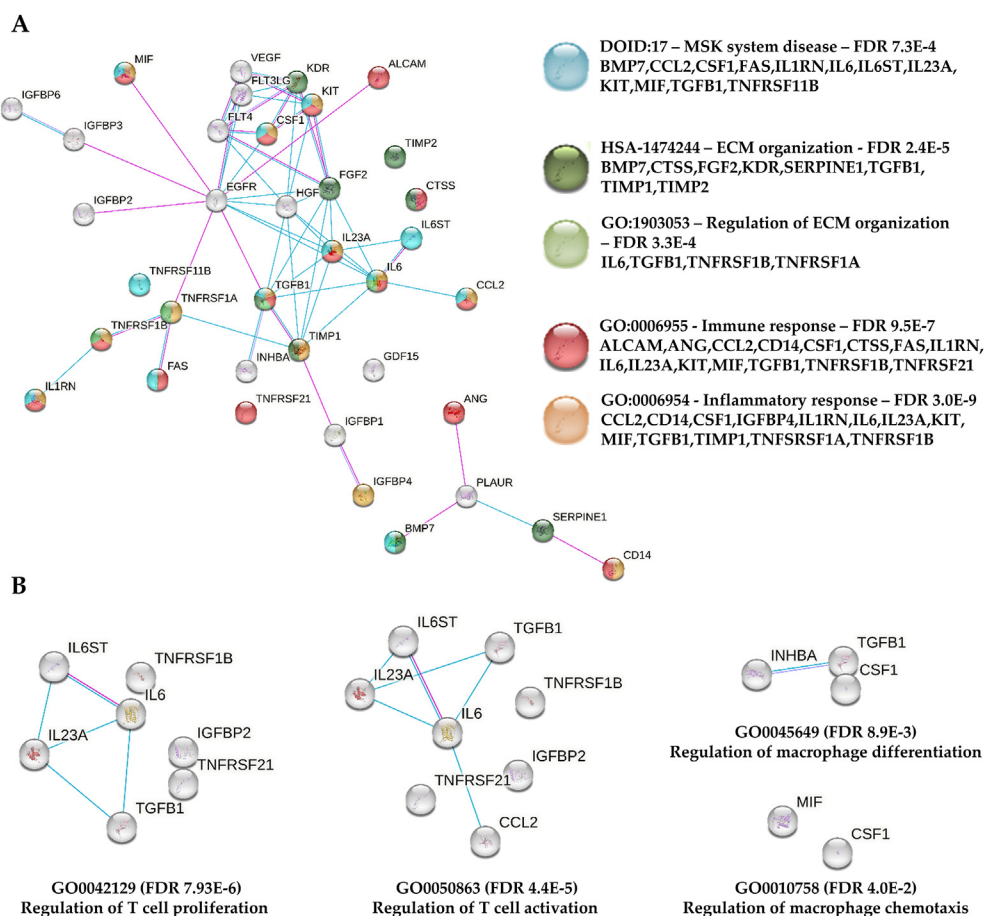
Fig. 2. Functional association network for identified secreted factors. A) Protein–protein interaction levels for 42 proteins shared in ASCs secretome, regardless culture medium, mined using STRING. Blue connections = proteins with known interactions based on curated databases; violet connections = proteins with experimentally determined interactions. Colourless nodes = proteins not related to the terms: MSK system disease, ECM organization, regulation of ECM organization, immune or inflammatory response. False discovery rate (FDR) for each term is also shown. Empty nodes = proteins of unknown 3D structure; filled nodes = known or predicted 3D structure. B) Protein–protein interaction networks for proteins belonging to regulation of T cell proliferation, activation and of macrophage differentiation, chemotaxis.

stimulatory molecules, such as CD80, CD83, and to a certain extent, CD86, with only a slight reduction observed at the highest concentration tested (data not shown). Furthermore, the expression of immunoregulatory macrophage marker M2, CD163, was significantly upregulated only in F compared to the control condition, with the most pronounced effects observed at the highest tested concentration (Fig. 7D). Again, X2 was the worst performer while X1 and H behaved similarly. Thus, F condition appeared to be have the highest immunomodulatory properties among the tested secretomes, followed by X1 and H while X2 seemed to lose the capacity to modulate monocyte polarization.

4. Discussion

In this work, a detailed characterization of adipose-MSCs secretome collected after culture in standard (FBS or hPL) and serum/xeno-free (two options ready for GMP translation) conditions was reported. Molecular analysis showed a dichotomy between molecules in the secretomes at both protein and exosome-shuttled miRNA levels. This difference was mirrored by divergent secretome effect on cell types related to osteoarthritis pathology, as chondrocytes and immune cells. Overall, secretomes of cells cultured in standard conditions appeared to have a higher anti-inflammatory and immunomodulatory potential. These observations are critically important considering that expanded cell culture

products for clinical applications are prepared using GMP-grade reagents and that to date there is a lack of specific evaluation of the true potency of these products.

The first divergence observed between standard and GMP culture conditions was in terms of cell density per area, with serum/xeno-free X1 and X2 having 3–5 fold higher values than FBS or hPL. This would have a double impact. First, a reduction of costs for both media/disposables and GMP structures where cells are produced. In a recent publication, cost estimates for cell-based therapies manufacturing ranged between €23K and €190K Euros per batch, with variable costs affecting total expenditure up to 87 % [29]. Second, under a biological perspective, higher cell number allows to reduce passages needed to obtain the requested amount of cells. This is of paramount importance for MSCs, since with high passage number a reduction in performance with increase of senescence was reported [30], including downregulation of expression levels of stem cell marker genes. Moreover, in ASCs an increase in DNA damage from the fifth passage onwards was reported indicating a possible mutagenic effect [31]. Of note, the genetic stability of MSCs expanded by GMP processes is a mandatory requisite [32] for clinical applications of both cells or derived products such as the secretome.

Alongside cell number, also the paracrine fingerprint of ASCs and their secretomes is crucial for therapeutic use. A proper modulation might drive their efficacy in relevant pathologies, with
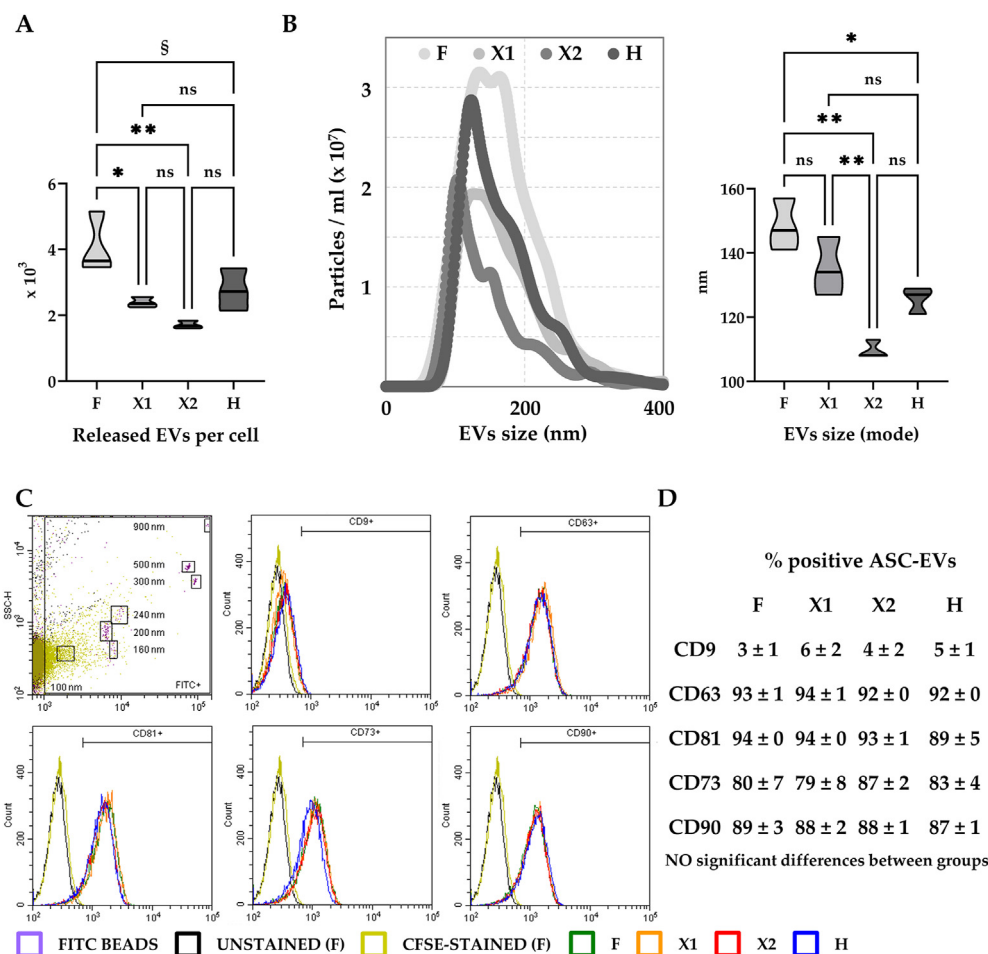
Fig. 3. ASC-EVs characterization. A) EVs released per cell calculated from NTA data. (median (thick line) and 25th and 75th quartiles, §p ≤ 0.10, *≤ 0.05, **≤ 0.01; N ≥ 3 independent experiments). B) EVs size analysis between conditions using NTA (each curve was obtained merging the data from three independent ASC lines). Mode size results are displayed as violin plots showing median (thick line) and 25th and 75th quartiles * for p ≤ 0.05, ** ≤ 0.01; N ≥ 3 independent experiments. C) Representative cytograms of EVs (CD9/63/81) and MSCs (CD73/90) markers tested in a representative ASC-EVs and superimposed in the dot plot with FITC-positive calibration beads of predetermined size (100, 160, 200, 240, 300, 500 and 900 nm) to confirm reliability of particle detection in the nanometric range. Unstained and CFSE stained samples represents only EVs from ASCs cultivated in FBS (condition F). D) Percentage of positive EVs for each marker (mean ± SD, N = 3 independent experiments).

musculoskeletal disorders and OA being among the most actively sifted in clinical trials [33] due to need of inflammation management and tissue homeostasis restoration [34]. In fact, even more importantly than their differentiation ability, it is now clear that MSCs, including ASCs, secrete bioactive factors that are immunomodulatory and trophic. For this reason, Arnold Caplan wisely suggested to change the name of MSCs to Medicinal Signaling Cells [9], in view of the ability of MSCs to interact with the resident cells within the microenvironment through signalling molecules. In this report, the array of soluble factors and EVs-associated miRNAs resulted affected by the culture medium used before secretome release. Regarding released proteins, the difference was less marked, with the most abundant proteins shared in their rankings by the four conditions. In this group (≥10,000 pg/10^6 ASCs), several factors related to OA emerged, as insulin-like growth factor (IGF)-binding proteins (IGFBPs) 3/4, vascular endothelial growth factor (VEGF) and tissue inhibitors of metalloproteinases (TIMPs) 1/2. If for VEGF and TIMPs clear pathologic [35] or protective [36] functions were reported, respectively, the role in OA of IGFBPs is still controversial. In fact, if IGF1 stimulates and maintains chondrocyte phenotype [37] and its masking by IGFBPs can reduce its availability to chondrocytes leading to cartilage deterioration [38], the same binding might protect IGF1 from degradation by increased protease

activity in the synovial fluid [39] allowing for a prolonged activity over time. Thus, overall, an increase of IGFBPs, by altering the bioavailability and function of IGFs, is likely to deliver IGFs-dependent and independent signals for chondrocyte survival. In the observed high similarity between conditions in terms of protein release, F emerged as the most diverging (lowest *r* value with respect to X1/2 and H), while few factors appeared significantly more abundant in X1, including IGFBP3, VEGF, TIMP2 and, in the 1000 to 10,000 pg/10^6 ASCs group, INHBA, PLAUR and GDF15. These proteins are related with OA, since INHBA is significantly increased in pathologic synovium [40] and cartilage [41], PLAUR is involved in activating matrix metalloproteinases to degrade proteoglycans [42] and GDF15 is a driver of senescence in chondrocytes and can contribute to OA progression by inducing angiogenesis [43]. Thus, although from these data it is not possible to drive a conclusive statement regarding soluble factors impact on OA, it may be postulated a less protective feature for those in the secretome collected after ASCs cultured in X1 medium.

A clearer picture emerged for EV-associated miRNAs, with a sharper dichotomy between FBS/hPL and serum/xeno free media. Of note, miR-24-3p, that was reported to attenuate IL1β-induced chondrocyte injury associated with OA [44] and promote M2 anti-inflammatory polarization of macrophages [45], resulted as the

Table 2
ASC-EVs released miRNAs after cultivation in the 4 media of the study.

miRNA	F	X1	X2	H	MEAN	F vs X1	F vs X2	F vs H	X1 vs X2	X1 vs H	X2 vs H	OA-RELATED FACTORS
miR-1183	2306	2691	90429	432	23964							
miR-24-3p	8161	9551	9254	6006	8243							IFNG,ADAM17,IL4,IL18,MMP14,TGFB1,CTSD,ANGPT2
miR-21-5p	10178	6753	2370	6696	6499		4.3 *					TGFB2,VEGFA,TIMP3,APC,TGFB1,MMP9,MMP2,WNT1
miR-125b-5p	10920	1223	280	6727	4787	8.9 ****	39.0 ****			0.2 **	0.04 **	IGF2,ANGPT2,IL1RL,APC,MMP13,LIF,EPO,MMP2,ADAMTS1
miR-222-3p	3119	1573	418	5151	2565		7.5 *			0.3 **	0.1 ***	KITLG,TIMP3,TIMP2,MMP1
miR-193b-3p	1288	3100	4360	1394	2536	0.4 **	0.3 ***			2.2 **	3.1 ***	PLAU,C5
miR-145-5p	2816	1356	749	3040	1990							ADAM17,MMP1,MMP14,IGF1,VEGFA,ANGPT2,TGFB2,FGF10
miR-19b-3p	1170	1712	2690	1726	1824		0.4 *					KITLG,CTGF,IGF1,TGFB1,PLAU
miR-100-5p	4076	264	408	2453	1800	15.5 ****	10.0 ****			0.1 ****	0.2 ****	IGF2,MMP13,MMP1
miR-99a-5p	3365	248	381	2613	1652	13.6 ****	8.8 ****			0.1 ***	0.1 ***	
miR-221-3p	1650	654	1530	2722	1639					0.2 *		TIMP3,MMP2,CXCL12
miR-214-3p	487	2784	2604	494	1592	0.2 **	0.2 **			5.6 **	5.3 **	CCL5,VEGFA,IGF1,ANGPT2
miR-92a-3p	506	1637	2652	970	1441	0.3 **	0.2 ****				2.7 ***	FGF2,CTSB,ADAMTS1
miR-194-5p	2	1690	3592	2	1321		0.0005 *				2391 *	
miR-150-5p	15	5	4862	1	1221							MMP14,VEGFA,IGF2
miR-31-5p	2082	444	123	1693	1086		16.9 ****			0.3 ***	0.1 ****	CXCL12,MMP3
miR-320a-3p	548	1266	1853	532	1050	0.4 **	0.3 ****			2.4 **	3.7 ***	
miR-132-3p	586	883	411	828	677							MMP13,FGF2,MMP9,BDNF
miR-574-3p	369	860	1006	309	636	0.4 **	0.4 ***			2.8 **	3.3 ***	TGFB1
miR-210-3p	802	615	312	568	574		2.6 *					BDNF,APC
miR-191-5p	410	585	852	417	566		0.5 *					BMP2
miR-484	160	1431	505	149	561					9.6 *		CTSD,IL2
miR-34a-5p	547	391	609	503	512							WNT1,MMP2,CD40LG,VEGFA,TGFB2,INHBB,
miR-30b-5p	406	509	609	297	455							CSF1
miR-20a-5p	348	422	392	649	452							CCL5,TIMP2,BMP2,VEGFA,PDGFB,FGF7
miR-199a-3p	605	366	199	492	415		3.0 **				0.4 *	FGF1,FGF7,HGF,VEGFA,FGF2,IGF1,EGF
miR-26a-5p	809	101	54	522	371	8.0 ****	14.9 ****			0.2 ****	0.1 ****	CTGF,HGF,IGF1,LIF
miR-29a-3p	448	200	77	649	343	2.2 **	5.8 ***			0.3 ****	0.1 ****	VEGFA,TGFB3,IGF1,MMP2,ADAMTS9,ADAM12
miR-30c-5p	288	403	443	222	339							CSF1,IL11,CTGF
miR-197-3p	141	287	517	148	273	0.5 **	0.3 ****				3.5 ****	IL18
miR-106a-5p	246	242	185	415	272						0.4 **	VEGFA,PDGFB,BMP2,TIMP2,APC,TGFB1,CCL5
miR-328-3p	114	378	477	118	272							
Let-7b-5p	684	73	61	235	263	9.4 **	11.2 **	2.9 *				PDGFB
miR-17-5p	220	251	205	361	259							MMP2,CCL5,TGFB1,TIMP3,BMP2,VEGFA,PDGFB
miR-224-5p	362	189	119	266	234		3.1 ***				0.4 *	
miR-152-3p	311	153	160	242	217	2.0 **						FGF2,WNT1,CSF1,ADAM17
miR-130a-3p	188	124	311	218	210				0.4 **			IGF1,TGFB1,IL18,CSF1,TNF
Let-7e-5p	539	44	47	177	202	12.4 ***	11.4 ***	3.0 **				TIMP3,PDGFB,IGF1,MMP9,WNT1
miR-193a-5p	171	190	97	265	181						0.4 ***	HGF
miR-99b-5p	416	44	30	221	178	9.5 ****	13.7 ****			0.2 **	0.1 **	
miR-138-5p	43	158	287	164	163		0.2 **					MMP3,TIMP1
miR-218-5p	62	107	252	62	121		0.2 *				4.1 *	APC,CTSB,MMP2,ADAM12,ADAM17
miR-16-5p	138	132	37	129	109							IFNG,BDNF,CTSD,FGF2,TIMP3,VEGFA,HGF
miR-106b-5p	90	94	144	91	105							IL4,MMP2,CCL5,APC,BMP2,VEGFA,PDGFB
miR-127-3p	179	40	15	156	97	4.5 ***	11.8 ***			0.3 **	0.1 ***	MMP13
miR-342-3p	60	150	66	94	93	0.4 *						
miR-376c-3p	78	75	159	56	92							
miR-10a-5p	222	16	8	100	87	13.8 ****	27.5 ****	2.2 **		0.2 *	0.1 *	MMP14,TGFB3,C5,BDNF
miR-143-3p	173	34	9	83	75	5.1 ****	18.3 ****	2.1 ***		0.4 *	0.1 **	PDGFB,CTGF,MMP14,MMP13,MMP9,MMP2,ADAMTS4,TNF

Table header groups: **A - pg/10⁹ ASC-EVs** (F, X1, X2, H, MEAN); **B - FOLD** (F vs X1, F vs X2, F vs H, X1 vs X2, X1 vs H, X2 vs H); **C - TARGETS** (OA-RELATED FACTORS).

Released ASC-EVs miRNAs ordered by mean, from most to less abundant factor, obtained from the four conditions. For each fold ≥ 2 or ≤ 0.5 the significance is shown: * for p-value ≤ 0.05, ** ≤ 0.01, $\leq$ *** 0.001 and **** ≤ 0.0001. N = 3.
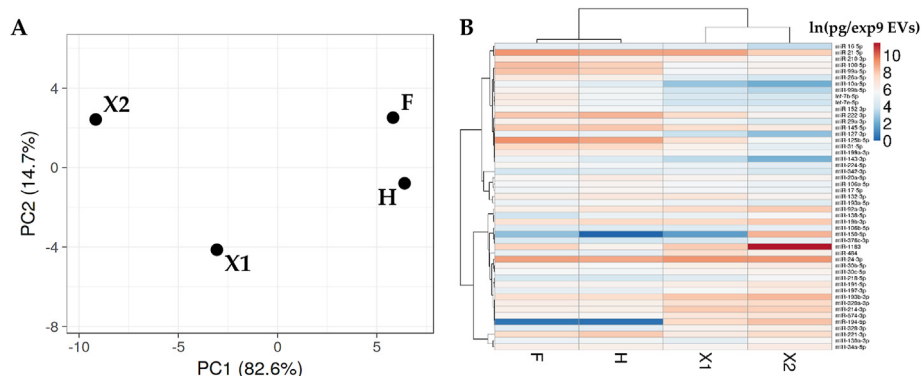
Fig. 4. Comparison of EV-miRNAs expression profiles in the first quartile of ASCs after expansion in the different media. (A) Principal component analysis of the ln transformed miRNA values expressed as pg per exp9 EVs (mean of the three ASC-EVs samples for each condition). X and Y axis show principal component 1 and principal component 2 that explain 82.6 % and 14.7 % of the total variance. (B) Heat map of hierarchical clustering analysis of ln transformed miRNA values expressed as pg per exp9 EVs (mean of the three ASC-EVs samples for each condition) with sample clustering tree at the top. Red shades = high expression levels; blue shades = low expression levels.

second most abundant molecule with no difference between conditions, after miR-1183 that has no reported roles for OA. Similarly, miR-21-5p, the third most abundant miRNA in this study results, which is reported to be negatively correlated with cartilage degeneration [46] and may change macrophage phenotype alleviating OA [47], was found significantly increased only in F *vs* X2. As evident in Table 2, almost all detected miRNAs were reported to experimentally target OA-related factors, thus suggesting how, globally, their presence confer protective features to ASCs EVs, as previously reported [48]. Nevertheless, many of the miRNAs in the first quartile of expression were more abundant after the expansion in presence of standard supplements (F/H). Among the top miRNAs (>1000 pg/10^9 EVs) following this pattern, we found miR-125b-5p, 222-3p, 100-5p, 99a-5p, 92a-3p and 31-5p. miR-125b-5p was reported as negative regulator of inflammatory genes in human OA chondrocytes [49] and inhibitor of T cell activation and cytotoxicity [50]. An inverse correlation of miR-222-3p with the OA radiographic severity score was found [51], possibly regulating cartilage erosion [52]. miR-100-5p in exosomes from intrapatellar fat pad-MSCs was able to protect articular cartilage *in vivo* [53] and its encapsulation in macrophage exosomes ameliorates synovial inflammation [50]. miR-99a-5p alleviates apoptosis and extracellular matrix degradation [54], alongside promoting macrophage autophagy [55] and inhibiting T helper type 1 (Th1) cell differentiation [56]. miR-92a-3p is an important regulator of matrix remodelling and inflammation in human chondrocytes [57], together with boosting Treg and dampening inflammatory T cell responses [58]. Eventually, miR-31-5p promotes chondrocytes homeostasis [59]. Thus, miRNAs with higher amount in EVs after F or H expansion might drive a protective function. Nevertheless, also 2 miRNAs in the >1000 pg/10^9 EVs group that are upregulated in X1/2 conditions were shown to have a protective effect on cartilage, miR-193b-3 [60] and 214-3p [61], while miR-320a family, including miR-320a-3p, was identified as potential diagnostic biomarker for fast-progressing OA [62]. Moreover, miR-214-3p can promote the differentiation of Treg cells and inhibit the polarization of M2 macrophages [63]. Thus, as for soluble factors it is difficult to drive a conclusive direction, although the preponderance of positive miRNA reduction in X1/X2 suggests a more protective role for F and H secretomes. This was supported by the analysis focused on single OA-related targeted factors in Table 3. A considerable number of inflammatory mediators, factors involved in cartilage sufferance and proteases affecting extracellular matrix (ECM) stability are hit at higher level by miRNAs in both F and H secretomes. In this group

lie OA-supporting pro-inflammatory cytokines such as Leukemia Inhibitory Factor (*LIF*, part of *IL6* family) [64], C-X-C Motif Chemokine Ligand 12 (*CXCL12*) [65] and tumour necrosis factor (*TNF*) [66], alongside ECM-degrading enzymes such as matrix metallopeptidases (*MMP1/2/3/13*) [67] and their activator APC Regulator of WNT signalling pathway (*APC*) [68], ADAM metallopeptidase with thrombospondin type 1 motif (*ADAMTS4/9*) [69] and a IL1 receptor (interleukin 1 receptor like 1, *IL1RL1*) [70]. Thus, albeit the presence of few pathogenic factors preferentially targeted by X1/X2 secretomes, the overall message for EV-miRNAs is a preponderance of protective signals in F and H conditions in a context of general safeguard given by ASCs released molecules.

This paradigm was supported by *in vitro* tests on chondrocytes and immune cells. On chondrocytes, all secretomes were able to reduce the inflammatory response elicited by IL1β. Medium H resulted in the strongest reduction for both ECM- (*CTSS*) and inflammation-related (*IL1/6/8*) genes, followed by F with good performance for *IL1* and *IL8*. The superior protective potential of standard media was confirmed with immune cells, especially for the ability to modulate the polarization of monocytes that have a crucial role in OA [71]. F secretome maintained the pro-monocytic marker CD14 expression, which is downregulated in mDCs, alongside a downregulation of differentiation marker CD1a. Furthermore, the expression of immunoregulatory macrophage marker M2, CD163, was upregulated at the highest tested concentration. This result is in agreement with the literature confirming ASCs [72], secretomes [73] and EVs [74] potential after culture in FBS to stimulate M2 macrophage polarization rather than reducing M1 markers. For the other media, the weakest regulation occurred with X2 condition while X1 and H had a similar response. Eventually, F secretome had again the best performance regarding T cell proliferation and polarization, followed by X1 and H, although statistical significance was very low or absent. Overall, these results are in agreement with a publication characterizing ASCs immunosuppressive potential when cultured with FBS, hPL or a serum/xeno-free medium identical to our condition X1 [75]. Likewise, Oikonomopoulos et al. who showed that FBS had the most positive effect on ASCs, followed by serum/xeno-free medium, while hPL exhibited diminished immunosuppressive properties, the results of the present study enlarge those finding that were mainly based on PBMSCs proliferation inhibition. Also, the overall different results on immune cells observed for X1 and X2 conditions, despite a similar secretory profile, corroborate previous findings in umbilical cord-MSCs where a different immunogenic capacity was dependent on the type of xeno/serum-free medium [76].

Table 3
OA-related factors targeted by ASC-EV miRNAs.

	A - pg/10^9 ASC-EVs (sum of factor targeting miRNAs)					B - FOLD						C - ROLE IN OA
	F	X1	X2	H	MEAN	F vs X1	F vs X2	F vs H	X1 vs X2	X1 vs H	X2 vs H	
CYTOKINES												
IL18	8490	9961	10082	6372	8726							Pro-inflammatory
IFNG	8299	9682	9291	6135	8352							Pro-inflammatory
IL4	8251	9645	9398	6098	8348							Anti-inflammatory
WNT1	11575	7341	3187	7619	7430		3.6 *					Overexpression of MMPs
LIF	11729	1323	334	7249	5159	8.9 ****	35.1 ****			0.2 **	0.05 ***	Pro-inflammatory
EPO	10920	1223	280	6727	4787	8.9 ****	39.0 ****			0.2 **	0.04 **	Progenitor induction
CXCL12	3732	1098	1653	4415	2725	3.4 **	2.3 **			0.2 ***	0.4 ***	Pro-inflammatory
CCL5	1391	3793	3529	2010	2681	0.4 **	0.4 ***					Pro-inflammatory
C5	1511	3116	4368	1494	2622							Proteoglycan and cartilage loss
CSF1	1193	1188	1523	979	1221							Pro-inflammatory, cartilage loss
IL2	160	1431	505	149	561					9.6 *		Pro-inflammatory
CD40LG	547	391	609	503	512							Pro-inflammatory
IL11	288	403	443	222	339							Pro-inflammatory
TNF	360	158	320	301	285	2.3 **			0.5 **			Pro-inflammatory
TNFSF11	90	94	144	91	105							Bone loss
GROWTH FACTORS												
TGFB1	20532	19493	16019	15731	17944							Cartilage matrix alteration
ANGPT2	22384	14913	12886	16267	16613							Pro-inflammatory
IGF1	15222	16237	15984	13324	15192							Cartilage anabolism
VEGFA	16136	12996	12431	13521	13771							Cartilage loss
TGFB2	13541	8500	3728	10239	9002		3.6 *					Cartilage matrix alteration
IGF2	15010	1491	5550	9181	7808	10.1 *						Cartilage anabolism
KITLG	4289	3285	3108	6877	4390					0.5 *	0.5 *	Synovial hyperplasia
FGF2	2146	3169	3459	2662	2859							Cartilage catabolism
CTGF	2440	2250	3196	2553	2610							Cartilage loss
FGF10	2816	1356	749	3040	1990							Anti-fibrotic
BMP2	1313	1595	1777	1933	1655							Chondrocyte anabolism
PDGFB	2126	1126	1034	1770	1514		2.1 **					Pathological angiogenesis
BDNF	1749	1645	768	1625	1447		2.3 ***		2.1 ***		0.5 ***	Chronic pain
HGF	1722	788	386	1408	1076		4.5 *					Bone remodelling
FGF7	952	787	591	1141	868							Oxidative stress
INHBB	547	391	609	503	512							Proliferation stimulator
TGFB3	670	216	85	749	430	3.1 ****	7.9 ****			0.3 ****	0.1 ****	Cartilage loss
EGF	605	366	199	492	415		3.0 **				0.4 *	Cartilage anabolism
FGF1	605	366	199	492	415		3.0 **				0.4 *	Cartilage loss
PROTEASES												
MMP2	24287	9707	5476	17895	14341	2.5 **	4.4 **				0.3 **	Matrix degradation
APC	22299	9034	3543	14559	12359	2.5 **	6.3 **				0.2 *	Activate MMPs
MMP14	11387	10962	14882	9230	11615							Matrix degradation
TIMP3	15845	9406	4607	15237	11274		3.4 **				0.3 *	Matrix protection
ADAM17	11350	11166	10415	9350	10570							Matrix degradation
CTSD	8459	11113	9795	6285	8913							Matrix degradation
MMP9	11477	7713	2838	7785	7453		4.0 *					Matrix degradation
MMP13	15934	2443	1123	10248	7437	6.5 ****	14.2 ****			0.2 ***	0.1 ***	Matrix degradation
PLAT	10178	6753	2370	6696	6499		4.3 *					Promote fibrinolytic activity
MMP1	10011	3193	1574	10644	6356	3.1 ***	6.4 ***			0.3 ***	0.1 ***	Matrix degradation
ADAMTS1	11426	2859	2932	7697	6229							Matrix degradation
IL1RL	10920	1223	280	6727	4787	8.9 ****	39.0 ****			0.2 **	0.04 **	IL1 receptor family
PLAU	2458	4813	7050	3121	4360		0.3 ****				2.3 ****	Promote fibrinolytic activity
TIMP2	3713	2237	994	6215	3290		3.7 *			0.4 **	0.2 ***	Matrix protection
CTSB	569	1744	2904	1031	1562	0.3 **	0.2 ****				2.8 ***	Matrix degradation
MMP3	2126	602	410	1857	1249	3.5 ***	5.2 ****			0.3 ***	0.2 ***	Matrix degradation
ADAM12	510	307	329	711	464					0.4 *		Matrix degradation
ADAMTS9	448	200	77	649	343	2.2 **	5.8 ***		2.6 *	0.3 ****	0.1 ****	Matrix degradation
TIMP1	43	158	287	164	163		0.2 **					Matrix protection
ADAMTS4	173	34	9	83	75	5.1 ****	18.3 ****	2.1 ***		0.4 **	0.1 ***	Matrix degradation

Released ASC-EVs miRNA targets ordered by mean, from most to less abundant factor, obtained from the four conditions. For each fold ≥2 or ≤0.5 the significance is shown: * for p-value ≤0.05, ** ≤0.01, ≤ *** 0.001 and **** ≤0.0001. N = 3.

This report has some limitations. First, to increase consistency between donors we opted to isolate ASCs from female donors of similar age. The possibility that gender differences could influence results is valid and merits consideration. In fact, albeit the core characteristics and functional properties of ASCs, such as multipotency, immunomodulation, and regenerative capacity, are largely consistent across individuals [77,78], some sex-specific transcriptomic differences were reported [79]. As we performed in this study, these differences may be minimized through standardized isolation, culture, and characterization protocols. Thus, while donor and gender differences are worth exploring, we believe that they do not undermine the reliability of the presented results, albeit future research will be needed to confirm herein reported findings. Second, the number of serum/xeno-free media used in the study was limited to only two options. The choice of focusing on GMP-ready or GMP-compliant alternatives was related to an easier and faster translation, being aware that several new products are already or will be on the market in the next years.
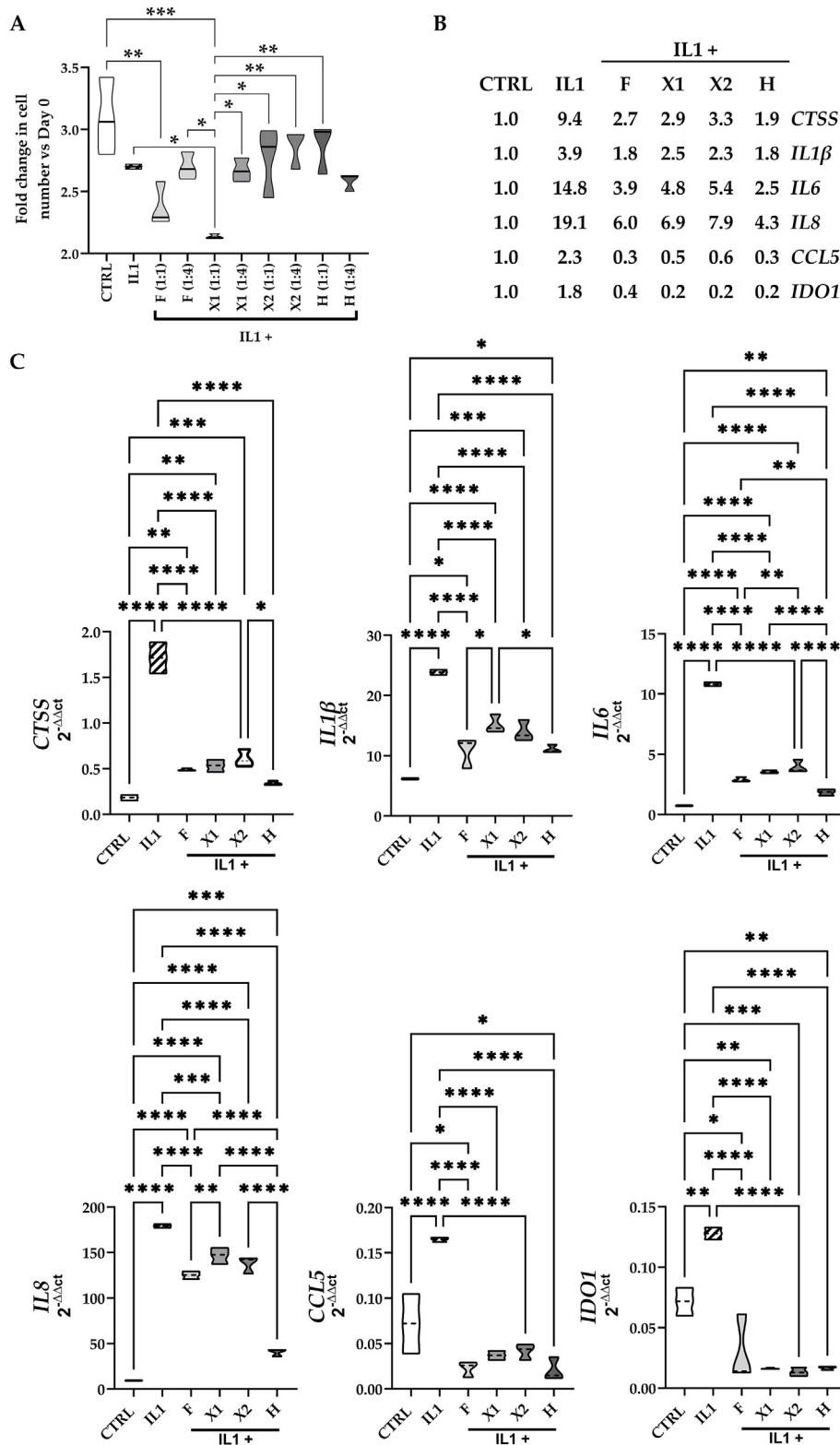
Fig. 5. Effect of secretomes on inflamed chondrocytes. A) Proliferation of chondrocytes exposed to IL1β with or without different dilutions of secretomes. (*p-value ≤0.05, **≤ 0.01; N = 3. B) Gene expression modulation (fold change *vs* CTRL set as 1) for chondrocytes exposed to IL1β without and with secretomes at 1:1 dilution. C) Single gene modulation (*p-value ≤0.05, **≤ 0.01, ***≤ 0.001 and ****≤ 0.0001; N = 3).

Related to expansion media, although ASCs were cultured for the same time and studied at the same passage, population doublings resulted higher in X1 and X2. To date, a direct correlation between the number of divisions and secretome fingerprint is not deeply investigated. For this reason, we opted to follow an expansion protocol relying on a reduced number of passages that was
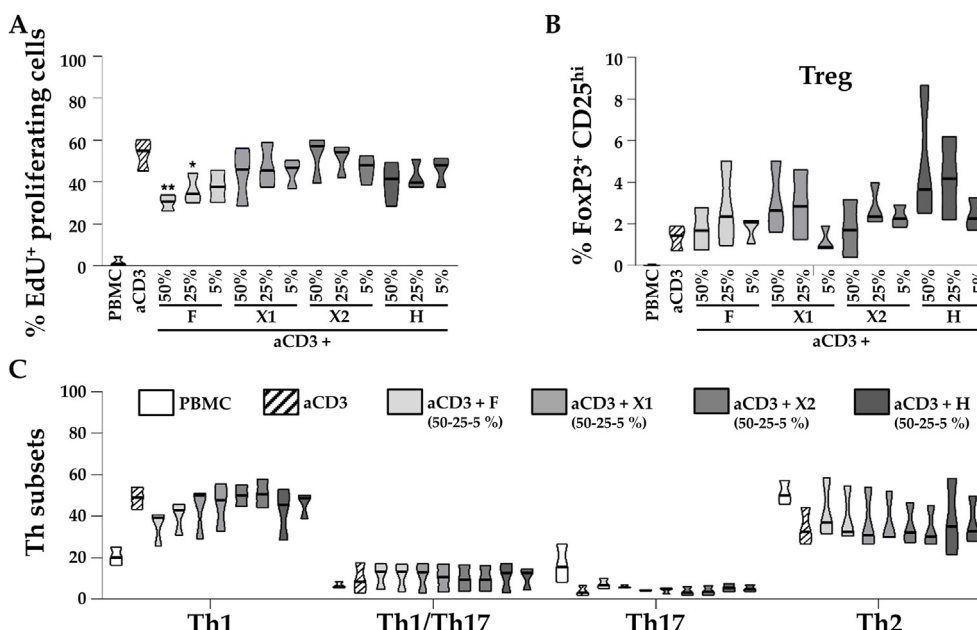
Fig. 6. Immunomodulatory effects of secretomes on PBMC proliferation and T lymphocytes differentiation. A) PBMCs proliferation (*p-value ≤0.05, ** ≤ 0.01 *vs* control (PBMC + anti-CD3), N = 3 independent experiments performed using 3 different PBMC donors and 3 different ASC secretome preparations). B) Treg induction. C) Th subsets differentiation.
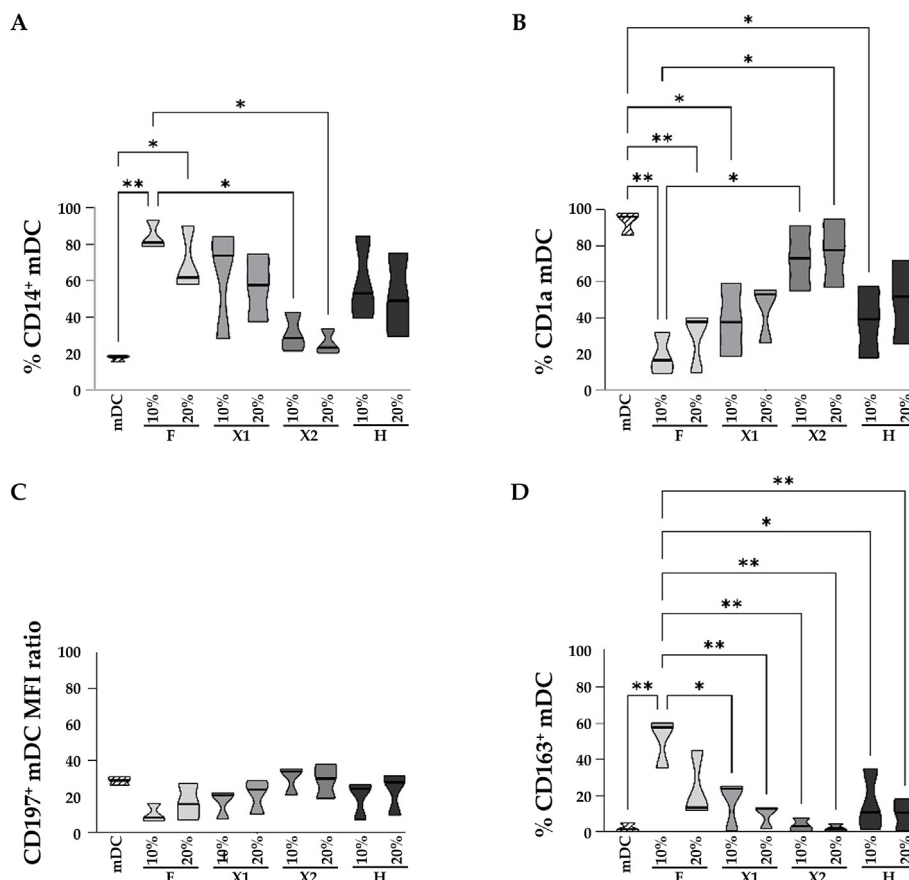
Fig. 7. Immunomodulatory effects of secretomes on monocyte differentiation toward antigen-presenting cells. The expressions of CD14 (A), CD1a (B) and CD197 (B) was assessed by flow cytometry to evaluate mDC differentiation. Furthermore, the expression of the macrophage type 2 marker, CD163 is presented (D). Results are presented as a percentage of expression or mean fluorescence intensity. mDC = mature Dentritic Cells; MFI = mean fluorescence intensity (calculated as the ratio between MFI of control and MFI of treated samples). *p-value ≤0.05, ** ≤0.01; N = 3 independent experiments performed using 3 different PBMC donors and 3 different ASC secretome preparations.

recently described for ASCs production under GMP [80]. We are aware that future studies linking secretome properties and population doublings rather than the number of passages are needed. Third, the array of molecules at both protein and miRNA levels was limited to a panel of 200 and 784 players. This allowed sifting among known factors possibly hiding undiscovered actors. We opted to characterize well-described molecules, most of which have a reported role for OA. In the next years, a more comprehensive analysis based on high-throughput NGS or proteomics will be mandatory. In fact, we are aware that for the OA-related factors that were reported in Tables 2C and 3A also other miRNAs than those herein tested might influence the overall amount and therefore potentially alter the balance between conditions we described. Moreover, a specific miRNA may regulate several mRNAs and a specific mRNA may be regulated by several miRNAs, suggesting that the total miRNA amount we proposed in Table 3A for a factor might be reduced if the single miRNAs contributing to the total value are reduced in their availability due to multiple bindings with other targets. Eventually, the *in vitro* test on chondrocytes and immune cells nicely supported the molecular signature of the different secretomes. These systems can just roughly recapitulate the secretome behaviour *in vivo* or in patients. The next step will be to focus the attention in animal models to refine the final message for the selection of the most optimal culturing conditions before testing in humans.

5. Conclusions

The data of this study indicate, in a context of similar molecular signature, a divergent fingerprint for ASCs secretomes when cultivated in standard FBS/hPL or GMP-grade serum/xeno-free conditions. This dichotomy was reflected on secretomes potential *in vitro* on cells involved in OA, such as chondrocytes, T cells and monocytes. Standard media resulted the most effective, with hPL being preferable for chondrocytes and FBS for immune cells. These data raise the question about the use of new media for MSCs expansion in clinical applications. While there are undeniable advantages for GMP-compliant processes, it suggests that a thorough and comprehensive characterization is necessary to evaluate the various MSC-specific products that are increasingly becoming available.

Ethics approval and consent to participate

The study was conducted in accordance with the Declaration of Helsinki, and approved by San Raffaele Hospital Ethics Committee ("Caratterizzazione e valutazione del potenziale rigenerativo delle cellule progenitrici tessuto specifiche ot-tenute da tessuto muscoloscheletrici", approval on date December 16th 2020, registered under number 214/int/2020 for surgery room waste material) and by Comitato Etico Provinciale di Brescia ("Studio delle proprietà immunomodulatorie di cellule e derivati placentari", approval on July 2nd 2020, registered under number NP 3968 for peripheral blood mononuclear cells). Informed consent was obtained from all subjects involved in the study.

Consent for publication

Not applicable. No participating patients may be identified.

Data availability

The datasets generated and/or analysed during the current study are available in the Open Science Framework repository, https://osf.io/c4gnv/?view_only=3e1594d867da4b128d9b0c60e7e6241f.

CRediT authorship contribution statement

Conceptualization, ER and AP; methodology, ER and AP; software, GG; validation, CC; formal analysis, MT, PDL, EV and PR; investigation, MT, PDL, EV and PR; resources, ER and AP; data curation, ARS; writing—original draft preparation, ER and AP; writing—review and editing, OP and LdG; visualization, ARS; supervision, OP and LdG; project administration, ER and AP; funding acquisition, OP and LdG. All authors have read and agreed to the published version of the manuscript.

Additional files

Additional file 1 (.xlsx): ASCs released factors in the different conditions per each donor expressed as pg/10^6 cells; Additional file 2 (.xlsx): ASCs EV-miRNAs in the different conditions per each donor expressed as pg/10^9 EVs; Additional file 3 (.xlsx): ASCs EV-miRNAs present in the first quartile of at least one of the twelve samples of the study, expressed as pg/10^9 EVs; Additional file 4 (.xlsx): Network analysis for validated target genes of first quartile EV-miRNAs.

Funding

Declaration of competing interests

The authors declare that they have no known competing financial interests or personal relationships that could have appeared to influence the work reported in this paper. All authors guarantee the originality of the study and ensure that it has not been published previously. All the listed authors have read and approved the submitted manuscript.

Acknowledgments

Appendix A. Supplementary data

Supplementary data to this article can be found online at https://doi.org/10.1016/j.reth.2025.01.016.

References

[1] Mavrogenis AF, Karampikas V, Zikopoulos A, Sioutis S, Mastrokalos D, Koulalis D, et al. Orthobiologics: a review. Int Orthop 2023. https://doi.org/10.1007/s00264-023-05803-z.

[2] Hunter DJ, Bierma-Zeinstra S. Osteoarthritis Lancet 2019. https://doi.org/10.1016/S0140-6736(19)30417-9.

[3] Huebner K, Frank RM, Getgood A. Ortho-biologics for osteoarthritis. Clin Sports Med 2019. https://doi.org/10.1016/j.csm.2018.09.002.

[4] Hohmann E, Tetsworth K, Glatt V. Is platelet-rich plasma effective for the treatment of knee osteoarthritis? A systematic review and meta-analysis of level 1 and 2 randomized controlled trials. Eur J Orthop Surg Traumatol 2020. https://doi.org/10.1007/s00590-020-02623-4.

[5] Kim KI, Kim MS, Kim JH. Intra-articular injection of autologous adipose-derived stem cells or stromal vascular fractions: are they effective for patients with knee osteoarthritis? A systematic review with meta-analysis of randomized controlled trials. Am J Sports Med 2023. https://doi.org/10.1177/03635465211053893.

[6] Bolia IK, Bougioukli S, Hill WJ, Trasolini NA, Petrigliano FA, Lieberman JR, et al. Clinical efficacy of bone marrow aspirate concentrate versus stromal vascular fraction injection in patients with knee osteoarthritis: a systematic review and meta-analysis. Am J Sports Med 2022. https://doi.org/10.1177/03635465211014500.

[7] Laver L, Filardo G, Sanchez M, Magalon J, Tischer T, Abat F, et al. The use of injectable orthobiologics for knee osteoarthritis: a European ESSKA-ORBIT consensus. Part 1-Blood-derived products (platelet-rich plasma). Knee Surg Sports Traumatol Arthrosc 2024. https://doi.org/10.1002/ksa.12077.

[8] Beaufils P. The use of injectable Orthobiologics for knee osteoarthritis: a formal ESSKA consensus. ESSKA. https://cdn.ymaws.com/www.esska.org/resource/resmgr/docs/consensus_projects/2024_orbit_complete_report.pdf. Accessed on 25th November 2024.

[9] Caplan AI. Mesenchymal stem cells: time to change the name. Stem Cells Transl Med 2017. https://doi.org/10.1002/sctm.17-0051.

[10] Lv Z, Cai X, Bian Y, Wei Z, Zhu W, Zhao X, et al. Advances in mesenchymal stem cell therapy for osteoarthritis: from preclinical and clinical perspectives. Bioengineering (Basel) 2023. https://doi.org/10.3390/bioengineering10020195.

[11] Shegos CJ, Chaudhry AF. A narrative review of mesenchymal stem cells effect on osteoarthritis. Ann Jt 2022. https://doi.org/10.21037/aoj-21-16.

[12] Sanz-Nogués C, O'Brien T. Current good manufacturing practice considerations for mesenchymal stromal cells as therapeutic agents. Biomater Biosyst 2021. https://doi.org/10.1016/j.bbiosy.2021.100018.

[13] Fitzgerald JC, Shaw G, Murphy JM, Barry F. Media matters: culture medium-dependent hypervariable phenotype of mesenchymal stromal cells. Stem Cell Res Ther 2023. https://doi.org/10.1186/s13287-023-03589-w.

[14] Jung S, Panchalingam KM, Rosenberg L, Behie LA. Ex vivo expansion of human mesenchymal stem cells in defined serum-free media. Stem Cell Int 2012. https://doi.org/10.1155/2012/123030.

[15] Becherucci V, Piccini L, Casamassima S, Bisin S, Gori V, Gentile F, et al. Human platelet lysate in mesenchymal stromal cell expansion according to a GMP grade protocol: a cell factory experience. Stem Cell Res Ther 2018. https://doi.org/10.1186/s13287-018-0863-8.

[16] Cimino M, Gonçalves RM, Barrias CC, Martins MCL. Xeno-free strategies for safe human mesenchymal stem/stromal cell expansion: supplements and coatings. Stem Cell Int 2017. https://doi.org/10.1155/2017/6597815.

[17] Palombella S, Perucca Orfei C, Castellini G, Gianola S, Lopa S, Mastrogiacomo M, et al. Systematic review and meta-analysis on the use of human platelet lysate for mesenchymal stem cell cultures: comparison with fetal bovine serum and considerations on the production protocol. Stem Cell Res Ther 2022. https://doi.org/10.1186/s13287-022-02815-1.

[18] Bhat S, Viswanathan P, Chandanala S, Prasanna SJ, Seetharam RN. Expansion and characterization of bone marrow derived human mesenchymal stromal cells in serum-free conditions. Sci Rep 2021. https://doi.org/10.1038/s41598-021-83088-1.

[19] Visconte C, Taiana MM, Colombini A, De Luca P, Ragni E, de Girolamo L. Donor sites and harvesting techniques affect miRNA cargos of extracellular vesicles released by human adipose-derived mesenchymal stromal cells. Int J Mol Sci 2024. https://doi.org/10.3390/ijms25126450.

[20] Marassi V, La Rocca G, Placci A, Muntiu A, Vincenzoni F, Vitali A, et al. Native characterization and QC profiling of human amniotic mesenchymal stromal cell vesicular fractions for secretome-based therapy. Talanta 2024. https://doi.org/10.1016/j.talanta.2024.126216.

[21] Szklarczyk D, Kirsch R, Koutrouli M, Nastou K, Mehryary F, Hachilif R, et al. The STRING database in 2023: protein-protein association networks and functional enrichment analyses for any sequenced genome of interest. Nucleic Acids Res 2023. https://doi.org/10.1093/nar/gkac1000.

[22] D'haene B, Mestdagh P, Hellemans J, Vandesompele J. miRNA expression profiling: from reference genes to global mean normalization. Methods Mol Biol 2012. https://doi.org/10.1007/978-1-61779-427-8_18.

[23] Huang HY, Lin YC, Cui S, Huang Y, Tang Y, Xu J, et al. miRTarBase update 2022: an informative resource for experimentally validated miRNA-target interactions. Nucleic Acids Res 2022. https://doi.org/10.1093/nar/gkab1079.

[24] Metsalu T, Vilo J. ClustVis: a web tool for visualizing clustering of multivariate data using Principal Component Analysis and heatmap. Nucleic Acids Res 2015. https://doi.org/10.1093/nar/gkv468.

[25] Chang L, Xia J. MicroRNA regulatory network analysis using miRNet 2.0. Methods Mol Biol 2023. https://doi.org/10.1007/978-1-0716-2815-7_14.

[26] Papait A, Ragni E, Cargnoni A, Vertua E, Romele P, Masserdotti A, et al. Comparison of EV-free fraction, EVs, and total secretome of amniotic mesenchymal stromal cells for their immunomodulatory potential: a

[27] translational perspective. Front Immunol 2022. https://doi.org/10.3389/fimmu.2022.960909.

Chou CH, Jain V, Gibson J, Attarian DE, Haraden CA, Yohn CB, et al. Synovial cell cross-talk with cartilage plays a major role in the pathogenesis of osteoarthritis. Sci Rep 2020. https://doi.org/10.1038/s41598-020-67730-y.

[28] Ragni E, De Luca P, Valli F, Zagra L, de Girolamo L. Inflammatory treatment used to mimic osteoarthritis and patients' synovial fluid have divergent molecular impact on chondrocytes in vitro. Int J Mol Sci 2023. https://doi.org/10.3390/ijms24032625.

[29] Ten Ham RMT, Hövels AM, Hoekman J, Frederix GWJ, Leufkens HGM, Klungel OH, et al. What does cell therapy manufacturing cost? A framework and methodology to facilitate academic and other small-scale cell therapy manufacturing costings. Cytotherapy 2020. https://doi.org/10.1016/j.jcyt.2020.03.432.

[30] Zhao AG, Shah K, Freitag J, Cromer B, Sumer H. Differentiation potential of early- and late-passage adipose-derived mesenchymal stem cells cultured under hypoxia and normoxia. Stem Cell Int 2020. https://doi.org/10.1155/2020/8898221.

[31] Guarnier LP, Moro LG, Lívero FADR, de Faria CA, Azevedo MF, Roma BP, et al. Regenerative and translational medicine in COPD: hype and hope. Eur Respir Rev 2023. https://doi.org/10.1183/16000617.0223-2022.

[32] Sensebé L, Gadelorge M, Fleury-Cappellesso S. Production of mesenchymal stromal/stem cells according to good manufacturing practices: a review. Stem Cell Res Ther 2013. https://doi.org/10.1186/scrt217.

[33] Law L, Hunt CL, van Wijnen AJ, Nassr A, Larson AN, Eldrige JS, et al. Office-based mesenchymal stem cell therapy for the treatment of musculoskeletal disease: a systematic review of recent human studies. Pain Med 2019. https://doi.org/10.1093/pm/pny256.

[34] Maldonado VV, Patel NH, Smith EE, Barnes CL, Gustafson MP, Rao RR, et al. Clinical utility of mesenchymal stem/stromal cells in regenerative medicine and cellular therapy. J Biol Eng 2023. https://doi.org/10.1186/s13036-023-00361-9.

[35] Nagao M, Hamilton JL, Kc R, Berendsen AD, Duan X, Cheong CW, et al. Vascular endothelial growth factor in cartilage development and osteoarthritis. Sci Rep 2017. https://doi.org/10.1038/s41598-017-13417-w.

[36] Mukherjee A, Das B. The role of inflammatory mediators and matrix metalloproteinases (MMPs) in the progression of osteoarthritis. Biomater Biosyst 2024. https://doi.org/10.1016/j.bbiosy.2024.100090.

[37] Goldring MB. The role of the chondrocyte in osteoarthritis. Arthritis Rheum 2000. https://doi.org/10.1002/1529-0131(200009)43:9<1916::AID-ANR2>3.0.CO;2-I.

[38] Galasso O, De Gori M, Nocera A, Brunetti A, Gasparini G. Regulatory functions of insulin-like growth factor binding proteins in osteoarthritis. Int J Immunopathol Pharmacol 2011. https://doi.org/10.1177/03946320110241S211.

[39] Rydén M, Turkiewicz A, Önnerfjord P, Tjörnstrand J, Englund M, Ali N. Identification and quantification of degradome components in human synovial fluid reveals an increased proteolytic activity in knee osteoarthritis patients vs controls. Proteomics 2023. https://doi.org/10.1002/pmic.202300040.

[40] Nanus DE, Badoume A, Wijesinghe SN, Halsey AM, Hurley P, Ahmed Z, et al. Synovial tissue from sites of joint pain in knee osteoarthritis patients exhibits a differential phenotype with distinct fibroblast subsets. EBioMedicine 2021. https://doi.org/10.1016/j.ebiom.2021.103618.

[41] Snelling S, Rout R, Davidson R, Clark I, Carr A, Hulley PA, et al. A gene expression study of normal and damaged cartilage in anteromedial gonarthrosis, a phenotype of osteoarthritis. Osteoarthritis Cartilage 2014. https://doi.org/10.1016/j.joca.2013.12.009.

[42] Wang Q, Shao G, Zhao X, Wong HH, Chin K, Zhao M, et al. Dysregulated fibrinolysis and plasmin activation promote the pathogenesis of osteoarthritis. JCI Insight 2024. https://doi.org/10.1172/jci.insight.173603.

[43] Weng PW, Pikatan NW, Setiawan SA, Yadav VK, Fong IH, Hsu CH, et al. Role of GDF15/MAPK14 Axis in chondrocyte senescence as a novel senomorphic agent in osteoarthritis. Int J Mol Sci 2022. https://doi.org/10.3390/ijms23137043.

[44] Xu J, Qian X, Ding R. MiR-24-3p attenuates IL-1β-induced chondrocyte injury associated with osteoarthritis by targeting BCL2L12. J Orthop Surg Res 2021. https://doi.org/10.1186/s13018-021-02378-6.

[45] Zhu F, Chen Y, Li J, Yang Z, Lin Y, Jiang B, et al. Human umbilical cord mesenchymal stem cell-derived exosomes attenuate myocardial infarction injury via miR-24-3p-promoted M2 macrophage polarization. Adv Biol (Weinh) 2022. https://doi.org/10.1002/adbi.202200074.

[46] Zhu H, Yan X, Zhang M, Ji F, Wang S. miR-21-5p protects IL-1β-induced human chondrocytes from degradation. J Orthop Surg Res 2019. https://doi.org/10.1186/s13018-019-1160-7.

[47] Qin L, Yang J, Su X, Li Xilan, Lei Y, Dong L, et al. The miR-21-5p enriched in the apoptotic bodies of M2 macrophage-derived extracellular vesicles alleviates osteoarthritis by changing macrophage phenotype. Genes Dis 2022. https://doi.org/10.1016/j.gendis.2022.09.010.

[48] Fan WJ, Liu D, Pan LY, Wang WY, Ding YL, Zhang YY, et al. Exosomes in osteoarthritis: updated insights on pathogenesis, diagnosis, and treatment. Front Cell Dev Biol 2022. https://doi.org/10.3389/fcell.2022.949690.

[49] Rasheed Z, Rasheed N, Abdulmonem WA, Khan MI. MicroRNA-125b-5p regulates IL-1β induced inflammatory genes via targeting TRAF6-mediated MAPKs and NF-κB signaling in human osteoarthritic chondrocytes. Sci Rep 2019. https://doi.org/10.1038/s41598-019-42601-3.

[50] Zhu Y, Zhang S, Li Z, Wang H, Li Z, Hu Y, et al. miR-125b-5p and miR-99a-5p downregulate human γδ T-cell activation and cytotoxicity. Cell Mol Immunol 2019. https://doi.org/10.1038/cmi.2017.164.

[51] Baloun J, Pekáčová A, Švec X, Kropáčková T, Horvathová V, Hulejová H, et al. Circulating miRNAs in hand osteoarthritis. Osteoarthritis Cartilage 2023. https://doi.org/10.1016/j.joca.2022.10.021.

[52] Song J, Jin EH, Kim D, Kim KY, Chun CH, Jin EJ. MicroRNA-222 regulates MMP-13 via targeting HDAC-4 during osteoarthritis pathogenesis. BBA Clin 2014. https://doi.org/10.1016/j.bbacli.2014.11.009.

[53] Wu J, Kuang L, Chen C, Yang J, Zeng WN, Li T, et al. miR-100-5p-abundant exosomes derived from infrapatellar fat pad MSCs protect articular cartilage and ameliorate gait abnormalities via inhibition of mTOR in osteoarthritis. Biomaterials 2019. https://doi.org/10.1016/j.biomaterials.2019.03.022.

[54] Wang Y, Zheng X, Luo D, Xu W, Zhou X. MiR-99a alleviates apoptosis and extracellular matrix degradation in experimentally induced spine osteoarthritis by targeting FZD8. BMC Muscoskel Disord 2022. https://doi.org/10.1186/s12891-022-05822-8.

[55] Wang G, Jing SY, Liu G, Guo XJ, Zhao W, Jia XL, et al. miR-99a-5p: a potential new therapy for atherosclerosis by targeting mTOR and then inhibiting NLRP3 inflammasome activation and promoting macrophage autophagy. Dis Markers 2022. https://doi.org/10.1155/2022/7172583.

[56] Gu Y, Zhou H, Yu H, Yang W, Wang B, Qian F, et al. miR-99a regulates CD4+ T cell differentiation and attenuates experimental autoimmune encephalomyelitis by mTOR-mediated glycolysis. Mol Ther Nucleic Acids 2021. https://doi.org/10.1016/j.omtn.2021.07.010.

[57] Mao G, Wu P, Zhang Z, Zhang Z, Liao W, Li Y, et al. MicroRNA-92a-3p regulates aggrecanase-1 and aggrecanase-2 expression in chondrogenesis and IL-1β-induced catabolism in human articular chondrocytes. Cell Physiol Biochem 2017. https://doi.org/10.1159/000484579.

[58] Fujiwara M, Raheja R, Garo LP, Ajay AK, Kadowaki-Saga R, Karandikar SH, et al. microRNA-92a promotes CNS autoimmunity by modulating the regulatory and inflammatory T cell balance. J Clin Invest 2022. https://doi.org/10.1172/JCI155693.

[59] Dai Y, Liu S, Xie X, Ding M, Zhou Q, Zhou X. MicroRNA-31 promotes chondrocyte proliferation by targeting C-X-C motif chemokine ligand 12. Mol Med Rep 2019. https://doi.org/10.3892/mmr.2019.9859.

[60] Chang ZK, Meng FG, Zhang ZQ, Mao GP, Huang ZY, Liao WM, et al. MicroRNA-193b-3p regulates matrix metalloproteinase 19 expression in interleukin-1β-induced human chondrocytes. J Cell Biochem 2018. https://doi.org/10.1002/jcb.26669.

[61] Cao Y, Tang S, Nie X, Zhou Z, Ruan G, Han W, et al. Decreased miR-214-3p activates NF-κB pathway and aggravates osteoarthritis progression. EBioMedicine 2021. https://doi.org/10.1016/j.ebiom.2021.103283.

[62] Ali SA, Espin-Garcia O, Wong AK, Potla P, Pastrello C, McIntyre M, et al. Circulating microRNAs differentiate fast-progressing from slow-progressing and non-progressing knee osteoarthritis in the Osteoarthritis Initiative cohort. Ther Adv Musculoskelet Dis 2022. https://doi.org/10.1177/1759720X221082917.

[63] Wang Q, Liu Y, Wu Y, Wen J, Man C. Immune function of miR-214 and its application prospects as molecular marker. PeerJ 2021. https://doi.org/10.7717/peerj.10924.

[64] Lotz M, Moats T, Villiger PM. Leukemia inhibitory factor is expressed in cartilage and synovium and can contribute to the pathogenesis of arthritis. J Clin Invest 1992. https://doi.org/10.1172/JCI115964.

[65] Xu Q, Sun XC, Shang XP, Jiang HS. Association of CXCL12 levels in synovial fluid with the radiographic severity of knee osteoarthritis. J Invest Med 2012. https://doi.org/10.2310/JIM.0b013e31825f9f69.

[66] Fernandes JC, Martel-Pelletier J, Pelletier JP. The role of cytokines in osteoarthritis pathophysiology. Biorheology 2002;39:237–46.

[67] Young DA, Barter MJ, Wilkinson DJ. Recent advances in understanding the regulation of metalloproteinases. F1000Res 2019. https://doi.org/10.12688/f1000research.17471.1.

[68] Jackson MT, Moradi B, Smith MM, Jackson CJ, Little CB. Activation of matrix metalloproteinases 2, 9, and 13 by activated protein C in human osteoarthritic cartilage chondrocytes. Arthritis Rheumatol 2014. https://doi.org/10.1002/art.38401.

[69] Li T, Peng J, Li Q, Shu Y, Zhu P, Hao L. The mechanism and role of ADAMTS protein family in osteoarthritis. Biomolecules 2022. https://doi.org/10.3390/biom12070959.

[70] Akhabir L, Sandford A. Genetics of interleukin 1 receptor-like 1 in immune and inflammatory diseases. Curr Genom 2010. https://doi.org/10.2174/138920210793360907.

[71] Nouri S, Feiz Barazandeh A, Ziyaeyan A, Viswanathan S. Understanding the different and contradictory roles of monocytes and macrophages in osteoarthritis. Cytotherapy 2024. https://doi.org/10.1016/j.jcyt.2024.03.401.

[72] Liu J, Qiu P, Qin J, Wu X, Wang X, Yang X, et al. Allogeneic adipose-derived stem cells promote ischemic muscle repair by inducing M2 macrophage polarization via the HIF-1α/IL-10 pathway. Stem Cell 2020. https://doi.org/10.1002/stem.3250.

[73] Yoon T, Ko E, Park Y. Secretome of adipose-derived mesenchymal stem cells establish anti-inflammatory milieu by developing M2b/c macrophage. J Immunol 2022. https://doi.org/10.4049/jimmunol.208.Supp.163.05.

[74] Heo JS, Choi Y, Kim HO. Adipose-derived mesenchymal stem cells promote M2 macrophage phenotype through exosomes. Stem Cell Int 2019. https://doi.org/10.1155/2019/7921760.

[75] Oikonomopoulos A, van Deen WK, Manansala AR, Lacey PN, Tomakili TA, Ziman A, et al. Optimization of human mesenchymal stem cell manufacturing: the effects of animal/xeno-free media. Sci Rep 2015. https://doi.org/10.1038/srep16570.

[76] Bobis-Wozowicz S, Kmiotek K, Kania K, Karnas E, Labedz-Maslowska A, Sekula M, et al. Diverse impact of xeno-free conditions on biological and regenerative properties of hUC-MSCs and their extracellular vesicles. J Mol Med (Berl) 2017. https://doi.org/10.1007/s00109-016-1471-7.

[77] Trotzier C, Bellanger C, Abdessadeq H, Delannoy P, Mojallal A, Auxenfans C. Deciphering influence of donor age on adipose-derived stem cells: in vitro paracrine function and angiogenic potential. Sci Rep 2024. https://doi.org/10.1038/s41598-024-73875-x.

[78] Vogt A, Faher A, Kucharczak J, Birch M, McCaskie A, Khan W. The effects of gender on mesenchymal stromal cell (MSC) proliferation and differentiation in vitro: a systematic review. Int J Mol Sci 2024. https://doi.org/10.3390/ijms252413585.

[79] Bianconi E, Casadei R, Frabetti F, Ventura C, Facchin F, Canaider S. Sex-specific transcriptome differences in human adipose mesenchymal stem cells. Genes 2020. https://doi.org/10.3390/genes11080909.

[80] Haack-Sørensen M, Mønsted Johansen E, Højgaard LD, Kastrup J, Ekblond A. GMP compliant production of a cryopreserved adipose-derived stromal cell product for feasible and allogeneic clinical use. Stem Cell Int 2022. https://doi.org/10.1155/2022/4664917.